university of groningen

faculty of science and engineering

Computing CMB Anisotropies in Compact Hyperbolic Universes

Author:
Utku Ercetin
(s4629701)

First Supervisor:
Prof dr. Marcello Seri
Second supervisor:
dr. Daan Meerburg
Daily Supervisor:
Robbert Scholtens

Bachelor's Thesis
To fulfill the requirements for the degree of
Bachelor of Science in Physics
at the University of Groningen

December 13, 2024

Contents

Abstract

The topology of the universe remains a fundamental question in cosmology, with compact hyperbolic 3-manifolds offering a compelling framework to explain anomalies in the cosmic microwave background (CMB) anisotropies. This thesis investigates the vibrational eigenmodes of such manifolds by solving the Laplace-Beltrami eigenvalue problem, $(\Delta + q^2)\Psi = 0$. Using the 'method of ghosts,' we attempt to numerically construct eigenfunctions on the universal cover H^3, ensuring invariance under the isometry group Γ, which acts freely and discontinuously on H^3 to yield the compact space M/Γ. Despite a meticulous implementation of the methodology outlined in [1], we were unable to replicate the reported numerical results for eigenvalues and their multiplicities. Our findings suggest the need for further refinement and validation of these methods to establish a robust computational framework for investigating compact hyperbolic manifolds.

Acknowledgements

I deeply appreciate the patience and understanding of both of my supervisors Marcello and Daan as I tried my best to make my way through this thesis. Although our initial idea didn't end up coming to much fruition in the end, I learned what it felt like to have to figure much of the content that was a part of the thesis on my own and rely on what I've learned to build a substantially large codebase. Not to mention that I now will look at any paper from the arXiv with much more scrutiny, since this one we examined was just a complete nightmare of typos, mistakes, and lack of explanations. I also thank Robbert Scholtens very much for being available to join our meetings and having answered many stupid questions Ive had along the way. I also deeply appreciate my family for giving me the opportunity to be able to complete two bachelors as a non-EU student, and always being there emotionally to console me through the times when I really felt like just not working those extra hours. Lastly I also thank my best friends, Miquel, Yuri, Nikola and Leo who supported me throughout the whole process and were there for me when I needed them.

1 Introduction

Human understanding of the universe has evolved from focusing on phenomena observable at everyday scales to exploring the extreme phenomena at the smallest and largest scales. This thesis focuses on efforts to comprehend the large-scale topology of the universe.

Data collected from missions such as COBE [2], WMAP [3], and Planck [4] suggests that the universe evolved according to the standard Big Bang model. In this framework, the time evolution of the geometry of local sections of the universe can be described by the Friedmann–Lemaître–Robertson–Walker (FLRW) metric [5, 6, 7]. This implies that the universe can be modeled as a 4-manifold, $\mathcal{U} = M \times \mathbb{R}$, where M is the 3-manifold corresponding to the spatial component, and $\mathbb{R}$ represents the temporal dimension. The FLRW metric arises from exact solutions to the Einstein field equations [8], resulting in a metric tensor g_{ij} that defines the distance element $ds^2 = g_{ij}dx^i dx^j$. Notably, the metric obeys the *cosmological principle*, which states that the universe is homogenous, isotropic and expanding, which is path connected but not necessarily simply-connected. Mathematically, while the metric tensor fixes the local geometric structure, it leaves the global topology ambiguous. A single metric tensor is consistent with numerous topologically distinct models.

The prevailing assumption in cosmology is that the universe is simply connected. While this assumption simplifies analysis, it is not necessarily justified. Proponents of this approach argue from a principle of economy, yet multi-connected models, which describe smaller and potentially finite universes, are equally valid. Under the assumption of constant curvature K, the simply connected possibilities for M are $\mathcal{S}^3$, E^3, and H^3, corresponding to $K = +1, 0, -1$, respectively. Relaxing the simply connected assumption introduces multi-connected models of the form $M = \tilde{M}/\Gamma$, where $\tilde{M}$ is one of $\mathcal{S}^3$, E^3, or H^3, and Γ is a group of isometries acting on $\tilde{M}$. This generalization also allows for finite models of the universe beyond the finite $\mathcal{S}^3$.

Recent work [9] emphasizes the observational significance of non-trivial topologies in negatively curved hyperbolic spaces (H^3). In the context of the concordonce model of cosmology, ΛCDM model, the assumption of a flat, simply connected topology (E^3) has explained many features of the cosmic microwave background (CMB) [10]. However, anomalies in the CMB, such as suppressed power at large angular scales, suggest the potential for multi-connected or hyperbolic universes [11, 12]. With by power here we refer to the square amplitude of temperature fluctuations at a given wavelength across the sky, which can be quantified in terms of angular scales through the multipole moments l. Large angular scales correspond to low l values, such as the quadrupole ($l = 2$) and octopole ($l = 3$) moments, which describe the largest structures observable in the CMB. These moments in the WMAP data display alignments and suppressions inconsistent with simple inflationary models, motivating the search for alternative cosmological topologies [12].

Compact hyperbolic spaces suppress large-scale temperature correlations by limiting the maximum observable distance and imposing a discrete set of eigenmodes for temperature fluctuations. Unlike infinite simply connected models, these spaces introduce a natural cutoff in correlation functions, meaning that temperature fluctuations on the largest scales are reduced. This suppression arises because the finite volume of compact hyperbolic spaces constrains the largest possible wavelengths of vibrational modes, thereby diminishing the power at low multi-

pole moments (l). This effect is similar to a small concert hall where only certain sound waves fit, suppressing deep bass notes because the space is too small for long wavelengths. Similarly, in compact hyperbolic spaces, the finite volume limits the largest possible temperature fluctuations, cutting off correlations at the largest scales.

The curvature K of the universe is determined by the total density parameter Ω_0, which measures the total energy density of the universe relative to the critical density $\rho_{\text{crit}} = \frac{3H^2}{8\pi G}$, where H is the Hubble parameter and G is the gravitational constant [13]. The total density parameter is defined as $\Omega_0 = \frac{\rho_{\text{tot}}}{\rho_{\text{crit}}}$, and it is related to the curvature through $K = H_0^2(\Omega_0 - 1)$, where $K > 0$ corresponds to a closed universe, $K = 0$ to a flat universe, and $K < 0$ to an open universe. Contributions to Ω_0 come from the matter density Ω_m, dark energy density Ω_Λ, radiation density Ω_r, and curvature density Ω_k, such that $\Omega_0 = \Omega_m + \Omega_\Lambda + \Omega_r + \Omega_k$. Deviations of Ω_0 from 1 indicate a curved universe, with $\Omega_k \neq 0$ [13].

To explore the implications of these multi-connected models, it is crucial to predict the CMB temperature fluctuations for these spaces. This requires solving the Laplace eigenvalue equation, $-\Delta\Psi = q^2\Psi$, on finite spaces. In this work, we attempt to replicate the numerical result of [1] to compute these eigenmodes and discuss their implementation and applications to cosmology.

2 Topology and Hyperbolic Manifolds

The concept of a manifold arises from the need to generalize the notion of a surface to higher dimensions, providing a mathematical framework to study spaces that locally resemble Euclidean space but can have complex global structures. Hyperbolic geometry was first developed in the 19th century by Lobachevsky and Bolyai as an alternative to Euclidean geometry, exploring the possible geometries which famously ignore Euclid's fifth postulate [14]. It describes spaces with constant negative curvature, where familiar geometric properties, such as the behavior of parallel lines or the growth of areas, are significantly different from the Euclidean case. Combining the ideas originating from hyperbolic geometry and the theory of manifolds gives rise to hyperbolic manifolds.

Using the key property of manifolds having global structures not necessarily resembling their local structures, we can explain the behavior of the global structure of the universe. Using already known results from Einstein and others for the local behavior, we can propose various models, the hyperbolic being one of these.

2.1 Manifolds

We introduce the concept of a manifold as a generalization of surfaces into higher dimensions as follows.

Definition 2.1

Let $(M, \mathcal{T})$ be a topological space. M is called a *topological manifold* of dimension n if:

- M is Hausdorff
- There exists $\mathcal{B} \subset \mathcal{T}$ such that any open in $\mathcal{T}$ can be written as a union of elements in $\mathcal{B}$
- For every point $p \in M$, there exists an open set $U \in \mathcal{T}$ containing p such that $U \cong \phi(U) = V \subset \mathbb{R}^n$

Wherein the pair (U, ϕ) is called a *chart*, U being the coordinate neighbourhood and $\phi : U \to \mathbb{R}^n$ the associated coordinate map.
We not also that by $\cong$ we mean an isomorphism.

The third condition is one of key importance, as this property is what gives the difference between local and global structures. A simple example which we can give is that of $\mathbb{S}^2$.

Example 2.2

Consider the 2-sphere, denoted by $\mathbb{S}^2 = \{(x, y, z) \in \mathbb{R}^3 \mid x^2 + y^2 + z^2 = 1\}$. While $\mathbb{S}^2$ is clearly a curved surface globally, we can describe it locally using charts that make it appear flat in a neighborhood of each point.
For instance, let $N = (0, 0, 1)$ and $S = (0, 0, -1)$ be the north and south poles of $\mathbb{S}^2$. Define two charts:

- The northern chart: $U_N = \mathbb{S}^2 \setminus \{N\}$, with the stereographic projection map $\phi_N : U_N \to \mathbb{R}^2$ defined by:

$$\phi_N(x, y, z) = \left(\frac{x}{1 - z}, \frac{y}{1 - z} \right).$$

- The southern chart: $U_S = \mathbb{S}^2 \setminus \{N\}$, with the stereographic projection map $\phi_S : U_S \to \mathbb{R}^2$ defined by:
$$\phi_S(x, y, z) = \left(\frac{x}{1+z}, \frac{y}{1+z} \right).$$

These charts cover the entire 2-sphere except for their respective poles, and locally map parts of $\mathbb{S}^2$ to subsets of $\mathbb{R}^2$. In these coordinate neighborhoods, the sphere appears locally 'flat' however, globally, the 'curvature' of $\mathbb{S}^2$ is preserved, demonstrating the distinction between local and global structures on a manifold. We put *flat*, and *curvature*, in this way since we have not yet defined what these mean in a mathematical context.

Now that we have this structure, we need also to see if it is possible to introduce some sort of smooth structure such that the concept of differentiation and tangency make sense. This is also necessary since in the wider context of the physics we want to look at, having smooth objects is almost required.

Definition 2.3

Let M be a topological manifold. A smooth atlas, $\mathcal{A}$, is a collection of charts (U_α, ϕ_α), for $\alpha \in I$ for I being some indexing set, where $U_\alpha \subset M$ are open sets and $\phi_\alpha : U_\alpha \to V_\alpha \subset \mathbb{R}^n$ are homeomorphisms, satisfying the following conditions:

- The collection of charts covers the entire manifold:
$$M = \bigcup_{\alpha \in I} U_\alpha.$$

- For any two overlapping charts (U_α, ϕ_α) and (U_β, ϕ_β) with $U_\alpha \cap U_\beta \neq \varnothing$, the transition map
$$\phi_\beta \circ \phi_\alpha^{-1} : \phi_\alpha(U_\alpha \cap U_\beta) \to \phi_\beta(U_\alpha \cap U_\beta)$$
is a diffeomorphism, i.e., it is bijective, smooth, and its inverse is smooth.

The charts in $\mathcal{A}$ are said to be *compatible*, as their transition maps satisfy these smoothness conditions, with two atlases, $\mathcal{A}_1$ and $\mathcal{A}_2$ being equivalent if their union is also a smooth atlas. Moreover, we call $\mathcal{A}$ a *smooth structure* on M if $\mathcal{A}$ also is an equivalence class of smooth atlases in M.

Now, it is indeed possible to give a definiton of a smooth manifold, the kind of manifolds with which we will be working on the most part in this paper.

Definition 2.4

An n-dimensional *smooth manifold* is a pair $(M, \mathcal{A})$ where M is a topological manifold and $\mathcal{A}$ is a smooth structure on M. Moreover, if the topology on M is compact, then we call M a *compact manifold*.

Example 2.5

Continuing with the example of $\mathbb{S}^2$, we will now show that it is a smooth manifold and also that it is compact.

First, as described earlier, the stereographic projection charts (U_N, ϕ_N) and (U_S, ϕ_S) provide a smooth atlas for $\mathbb{S}^2$. To verify smoothness, consider the transition maps between overlapping regions of the charts. For points in the intersection $U_N \cap U_S$, the transition

map $\phi_S \circ \phi_N^{-1}$ maps $\phi_N(U_N \cap U_S) \subset \mathbb{R}^2$ to $\phi_S(U_N \cap U_S) \subset \mathbb{R}^2$, and is explicitly given by:

$$\phi_S \circ \phi_N^{-1}(u, v) = \left(\frac{u}{u^2 + v^2}, \frac{v}{u^2 + v^2} \right),$$

where $(u, v) \in \mathbb{R}^2$ are coordinates in $\phi_N(U_N \cap U_S)$. This map is smooth, as it is composed of rational functions that are differentiable everywhere their denominator is nonzero, which is the case here since $u^2+v^2 > 0$ in the domain of ϕ_N. Similarly, its inverse, $\phi_N \circ \phi_S^{-1}$, is smooth.

Since the transition maps are smooth, the charts are compatible, and the atlas $\mathcal{A} = \{(U_N, \phi_N), (U_S, \phi_S)\}$ defines a smooth structure on $\mathbb{S}^2$. Therefore, $\mathbb{S}^2$ is a smooth manifold.

Next, to verify compactness, recall that $\mathbb{S}^2$ is the set $\{(x, y, z) \in \mathbb{R}^3 : x^2 + y^2 + z^2 = 1\}$, which is both closed and bounded in $\mathbb{R}^3$. By the Heine-Borel theorem, any subset of $\mathbb{R}^n$ that is closed and bounded is compact. Therefore, $\mathbb{S}^2$ is compact.
In conclusion, $\mathbb{S}^2$ is a compact smooth manifold.

Having established that $\mathbb{S}^2$ is a compact smooth manifold as a motivating example, we now turn to an important construct that arises naturally in the study of manifolds: the vector bundle. A vector bundle allows us to associate a vector space to each point of a manifold in a smooth and consistent way, enabling the study of geometric and algebraic structures that vary over the manifold.

For instance, at each point $p \in M$, the tangent space T_pM captures the local linear structure of the manifold, consisting of all possible directions in which one can move away from p. The smooth assembly of these tangent spaces across M forms the tangent bundle, a foundational example of a vector bundle. While we will not explore the tangent bundle in detail here, the interested reader can refer to standard texts on differential geometry [15] for a deeper treatment of tangent spaces and their role in smooth manifolds.

With this context, we now proceed to the general definition of a vector bundle, which extends the idea of smoothly varying vector spaces to a broader setting.

Definition 2.6

Let E, M be manifolds, and $\pi : E \to M$ be a continuous, surjective mapping between them. Then, (E, M, π) is an n-dimensional *vector bundle* over M if, for all $p \in M$,

1. the *fibre* $E_p = \pi^{-1}(p)$ is an n-dimensional vector space.
2. there exists a pair, $(\pi^{-1}(U), \phi)$, called a *bundle chart*, with U an open neighbourhood of p, and ϕ being the mapping $\phi : \pi^{-1}(U) \mapsto U \times \mathbb{R}$ such that when we restrict onto a single fibre, picking any $u \in U$, $\phi|_{E_u} : E_u \mapsto \{u\} \times \mathbb{R}^n$ is an isomorphism of vector spaces.

Definition 2.7

Let M be a smooth manifold of dimension m. The *tangent bundle* of M, denoted by TM, is the vector bundle (TM, M, π) where:

1. The total space $TM = \bigsqcup_{p \in M} T_pM$ is the disjoint union of the tangent spaces T_pM at all points $p \in M$. Each T_pM is an m-dimensional vector space.

2. The base space is the manifold M.

3. The projection map $\pi : TM \to M$ sends each tangent vector $v \in T_pM$ to the point p, i.e., $\pi(v) = p$.

4. For each point $p \in M$, there exists a *bundle chart* $(\pi^{-1}(U), \phi)$, where $U \subseteq M$ is an open neighborhood of p and $\phi : \pi^{-1}(U) \to U \times \mathbb{R}^m$ is a homeomorphism. Moreover:

$$\phi|_{T_qM} : T_qM \to \{q\} \times \mathbb{R}^m$$

is a linear isomorphism of vector spaces for each $q \in U$.

Moreover, a continuous mapping $\Gamma : M \to TM$ is called a *section* of the bundle, if $\pi \circ \Gamma(p) = p$ for all $p \in M$. A smooth section[1] of the bundle is a *vector field*. The set of all vector fields on the tangent bundle, is denoted as $\mathfrak{X}(M)$.

By smoothly associating vector spaces to points of a manifold, vector bundles provide a framework for analyzing and constructing structures that are both local and global in nature. For instance, sections of a vector bundle, such as vector fields, allow us to study the dynamics and geometry of manifolds through algebraic and analytical tools.

We now generalize this concept to tensors, which extend the idea of multilinear mappings on vector spaces. These objects allow us to encode and manipulate more complex structures, bridging the local geometry of tangent bundles with global properties of manifolds.

Definition 2.8
Let V be an n-vector space, and V^* its dual. Then, the multilinear map, τ,

$$\tau : V^* \times \ldots \times V^* \times V \times \ldots \times V \to \mathbb{R}$$

is called a *tensor* of type (r, s), r-contra, s-co (variant). Moreover, we may define the space of type (r, s) tensors with a real vector space structure as

$$T^r_s(V) := Mult(V^*, \ldots, V^*, V, \ldots, V)$$

Moreover, we equip the space of tensors with the *tensor product* as such: Let $\tau_1 \in T^r_s(V)$ and $\tau_2 \in T^{r'}_{s'}$ be tensors. Then, we define the *tensor product* of τ_1 and τ_2, $\tau_1 \otimes \tau_2$, as the $(r + r', s + s')$-tensor via

$$\tau_1 \otimes \tau_2(\omega^1, \ldots \omega^{r+r'}, v_1, \ldots v_{s+s'}) = \tau_1(\omega^1, \ldots \omega^r, v_1, \ldots, v_s) + \tau_2(\omega^{r+1}, \ldots \omega^{r'}, v_{s+1}, \ldots, v_{s'})$$

This equips the space of tensors with the product

$$\bigotimes : T^r_s(V) \times T^{r'}_{s'}(V) \to T^{r+r'}_{s+s'}(V)$$

Now, much like how the smooth sections of the tangent bundle corresponded to what we called vector fields, we can do the same with examining the smooth sections of the tensor bundle.

[1] See [16] for details on smooth structures on vector bundles

Definition 2.9

The (r, s)-tensor bundle over M is the vector bundle over tensor spaces with the base vector space being the tangent space of the base manifold, $(T^r_s(M),\, M,\, \pi)$. Namely,

$$T^r_s(M) := \bigsqcup_{p\in M} (\{p\} \times T^r_s(T_pM))$$

where $\pi : T^r_s(M) \to M$. A section of the tensor bundle, $\Gamma(T^r_s M)$ of $T^r_s(M)$ i.e. a smooth map $\tau. : M \to T^r_s(M)$ which statisfies the section property, is called a *tensor field* of type (r, s). The space of tensor fields is as $\mathcal{T}^r_s(M)$, where we set $\mathcal{T}^0_0(M) := C^\infty(M)$.

Example 2.10

Continuing with the example of $\mathbb{S}^2$, we now consider its tangent bundle, which is a fundamental example of a vector bundle. At each point $p \in \mathbb{S}^2$, viewed as a vector in $\mathbb{R}^3$, the tangent space $T_p\mathbb{S}^2$ consists of all vectors in $\mathbb{R}^3$ that are tangent to $\mathbb{S}^2$ at p. Formally, this is the subspace of $\mathbb{R}^3$ defined by

$$T_p\mathbb{S}^2 = \{v \in \mathbb{R}^3 : v \cdot p = 0\},$$

where $v \cdot p$ denotes the Euclidean dot product. This condition ensures that v is orthogonal to the normal vector at p, confining v to the tangent plane at p.
To define the tangent bundle $T\mathbb{S}^2$, we consider the disjoint union of all tangent spaces:

$$T\mathbb{S}^2 = \bigsqcup_{p\in\mathbb{S}^2} T_p\mathbb{S}^2.$$

The projection map $\pi : T\mathbb{S}^2 \to \mathbb{S}^2$ sends each tangent vector $v \in T_p\mathbb{S}^2$ to its base point p. It is not hard to verify that the pair $(T\mathbb{S}^2, \mathbb{S}^2, \pi)$ satisfies the definition of a vector bundle.

To illustrate, consider a smooth vector field on $\mathbb{S}^2$, which is a smooth section of the tangent bundle $T\mathbb{S}^2$. An example of such a vector field is the rotational vector field corresponding to rotations about the z-axis. In spherical coordinates (θ, ϕ), where θ is the polar angle and ϕ is the azimuthal angle, this vector field can be written as:

$$X(\theta, \phi) = \frac{\partial}{\partial\phi}.$$

This means that at each point on $\mathbb{S}^2$, the vector $X(\theta, \phi)$ is tangent to the sphere and points in the direction of increasing azimuthal angle ϕ. The smoothness of X follows from the smooth dependence of its components on the coordinates (θ, ϕ). Thus, X serves as a concrete example of a smooth section of $T\mathbb{S}^2$, demonstrating how vector fields encode smoothly varying directions on a manifold.

Definition 2.11

Let M be a smooth manifold of dimension n. A *metric tensor* on M is a symmetric, positive-definite, $(0, 2)$-tensor field g, defined as:

$$g : \mathfrak{X}(M) \times \mathfrak{X}(M) \to \mathbb{R}, \tag{2.1}$$

where $\mathfrak{X}(M)$ denotes the space of smooth vector fields on M, and $C^\infty(M)$ is the space of smooth real-valued functions on M, satisfying the following properties: Let $X, Y, Z \in \mathfrak{X}(M)$ and $f \in C^\infty(M)$, then

- $g(fX + Y, Z) = fg(X, Z) + g(Y, Z)$, and similarly for the second argument.
- $g(X, Y) = g(Y, X)$.
- $g(X, X) \geq 0$, with equality if and only if $X = 0$.

In local coordinates (x^i) on M, the metric tensor g is expressed as:

$$g = \sum_{i,j=1}^{n} g_{ij}(x)\, dx^i \otimes dx^j = g_{ij}(x)\, dx^i \otimes dx^j,$$

where, $g_{ij}(x) = g\left(\frac{\partial}{\partial x^i}, \frac{\partial}{\partial x^j}\right)$ are the components of the metric tensor in the coordinate basis anddx^i are the dual basis 1-forms[2].

Given a metric on a manifold with which we want to work, the notion of measuring distance between any two points on it is now natural. Specifically, the metric tensor g allows us to define the length of curves on the manifold, which can then be used to determine the shortest path, or geodesic, between two points.

Mathematically, the distance between two points $p, q \in M$ is defined using the infimum of the lengths of all smooth curves connecting p to q. If $\gamma : [a, b] \to M$ is a smooth curve parameterized by t, its length is given by:

$$L(\gamma) = \int_a^b \sqrt{g(\dot\gamma(t), \dot\gamma(t))}\, dt,$$

where $\dot\gamma(t)$ is the tangent vector to γ at t, and $g(\dot\gamma(t), \dot\gamma(t))$ is the squared norm of this vector as determined by the metric tensor g. The distance function $d : M \times M \to \mathbb{R}$ is then defined as:

$$d(p, q) = \inf_\gamma L(\gamma), \tag{2.2}$$

where the infimum is taken over all smooth curves γ such that $\gamma(a) = p$ and $\gamma(b) = q$.

Example 2.12

Consider $\mathbb{S}^2$ with the standard round metric induced from the Euclidean metric in $\mathbb{R}^3$. In spherical coordinates (θ, ϕ), the metric tensor g is given by:

$$g = d\theta^2 + \sin^2\theta\, d\phi^2.$$

The length of a curve $\gamma(t) = (\theta(t), \phi(t))$ on $\mathbb{S}^2$ is:

$$L(\gamma) = \int_a^b \sqrt{\left(\frac{d\theta}{dt}\right)^2 + \sin^2\theta \left(\frac{d\phi}{dt}\right)^2}\, dt.$$

To compute the distance between two points $p, q \in \mathbb{S}^2$, one would find the shortest such

[2]See [16] for more information on differential forms

curve, which in this case corresponds to a great circle arc connecting p and q. The distance $d(p, q)$ is thus given by:

$$d(p, q) = R\,\Delta\sigma,$$

where R is the radius of the sphere (assumed to be 1 here) and $\Delta\sigma$ is the central angle between p and q as measured from the origin in $\mathbb{R}^3$. For the unit sphere, this simplifies to:

$$d(p, q) = \arccos(p \cdot q),$$

where $p, q \in \mathbb{R}^3$ are the Euclidean coordinates of the points, and the dot product $p \cdot q$ measures their angular separation.

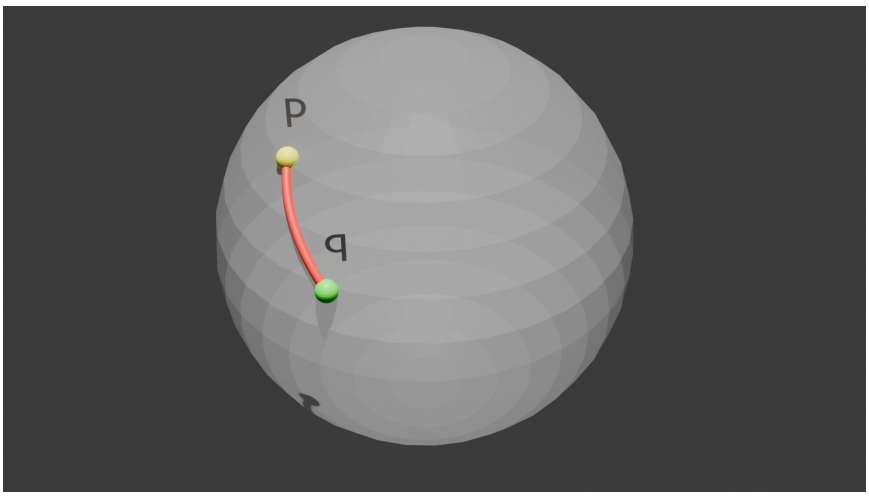

Figure 1: Geodesic between random points p, q on the sphere. Geodesics on the sphere are arcs of great circles.

Although the above example is relatively simple, we will see that this concept of distance is crucial. Then, given this idea of distance, we can define the following

Definition 2.13

An *isometry* is a distance-preserving transformation between metric spaces. An isometry is a diffeomorphism $f : M \to M$ such that for any two points $x, y \in M$, the hyperbolic distance remains unchanged:

$$d_M(f(x), f(y)) = d_M(x, y).$$

The collection of all such isometries forms a group under composition, known as the *isometry group* of M.

The idea of an isometry group will tie into our discussion on hyperbolic manifolds later as transformations which will leave our space invariant in certain ways, for example by preserving distances. Nonetheless, to tie together this concept of the metric with a manifold, we define the following

Without going too much into detail about curvature on manifolds, we briefly outline the essential concepts. Curvature on a Riemannian manifold is a measure of how the geometry deviates from being flat, as defined by the Euclidean geometry of $\mathbb{R}^n$. A key object used to quantify this is the Riemann curvature tensor, which encodes the failure of parallel transport around infinitesimal loops to be path-independent.

The sectional curvature is a scalar quantity derived from the Riemann curvature tensor [17]. In particular, given a point $p \in M$ and a 2-dimensional subspace $(X, Y) \in \sigma \subset T_pM$, the sectional curvature $K(\sigma)$ is defined as:

$$K(X,Y) = \frac{g(R(X,Y)Y,X)}{\|X\|^2\|Y\|^2 - g(X,Y)^2},$$

where R is the Riemann curvature tensor, and X, Y are linearly independent vectors spanning σ.

When the sectional curvature is constant, it takes the same value K for all 2-dimensional subspaces σ at every point on the manifold. For hyperbolic manifolds, the constant sectional curvature K is negative, indicating that the geometry is intrinsically 'saddle-shaped'. This contrasts with positive curvature, as found in spheres, and zero curvature, as found in flat Euclidean spaces.

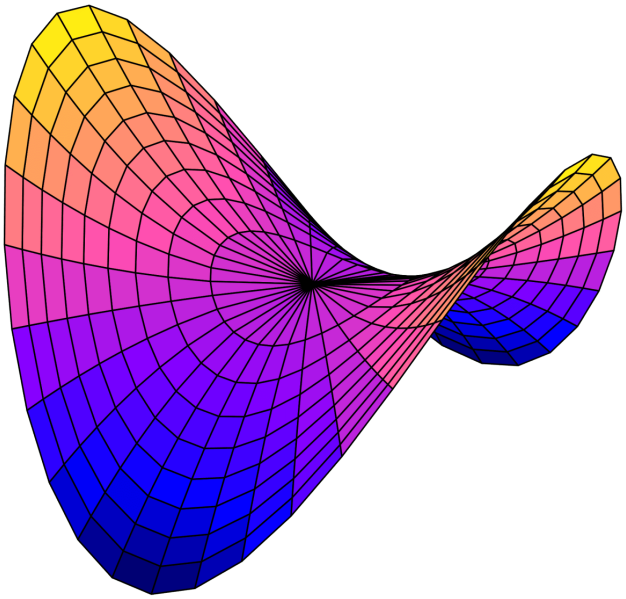

Figure 2: The saddle-shaped geometry of hyperbolic space. At every point, the surface curves in opposite directions. Figure from [18].

Definition 2.14

A *Riemannian manifold* is a smooth manifold M equipped with a metric tensor g, (M, g). If M has constant negative sectional curvature, it is called a *hyperbolic manifold*.

Thus, a hyperbolic manifold is a Riemannian manifold whose intrinsic geometry reflects the properties of spaces with constant negative curvature, such as the hyperbolic plane H^2 or its higher-dimensional analogue. For now we leave the discussion of hyperbolic spaces for after we define indeed what hyperbolic space is.

2.2 Covering Spaces

In the study of topology and geometry, covering spaces play a fundamental role in understanding the global properties of spaces by examining their local structures. Before delving into covering spaces, we recall some essential concepts related to connectedness in topological spaces.

Definition 2.15

A topological space X is said to be *simply connected* if:

1. X is path-connected; that is, for any two points $x, y \in X$, there exists a continuous map $\gamma : [0,1] \to X$ such that $\gamma(0) = x$ and $\gamma(1) = y$.
2. Every loop in X can be continuously contracted to a single point.

Simply connected spaces have no 'holes' in the sense that every closed loop can be shrunk to a point within the space. This property is significant in many areas of mathematics, including complex analysis and algebraic topology, as it often simplifies the analysis of functions and mappings on the space.

Definition 2.16

A topological space X is said to be *multi-connected* if it is connected but not simply connected. This means there exist loops in X that cannot be continuously contracted to a single point.

Multi-connected spaces possess a richer topological structure due to the presence of non-contractible loops. These loops represent 'holes' or 'handles' in the space, leading to interesting phenomena in their topological and geometric properties.

Example 2.17

An illustrative example of a multi-connected space is the torus $T^2 = S^1 \times S^1$. The torus, being the product of two circles, has a doughnut-like shape with two independent directions in which loops cannot be contracted. This structure makes it a fundamental object of study in topology and geometry.

To analyze such spaces, we introduce the concept of covering spaces, which allows us to "lift" paths and loops to a space where they can be more easily understood.

Definition 2.18

Let X be a topological space. The pair $(\tilde{X}, p)$, where $\tilde{X}$ is a topological space and $p : \tilde{X} \to X$ is a continuous surjective map, is called a *covering space* or *cover* of X if, every point $x \in X$ has an open neighborhood $U \subset X$ such that $p^{-1}(U)$ can be expressed as a disjoint union of open sets, each of which is mapped homeomorphically onto U by p.

Moreover, if $\tilde{X}$ is simply connected, then it is called the *universal cover* of X.

Covering spaces enable us to study the local behavior of a space X by examining the simpler space $\tilde{X}$. This approach is particularly useful when $\tilde{X}$ is simply connected, as it allows for the lifting of paths and homotopies from X to $\tilde{X}$, simplifying many problems.

Example 2.19

Consider the real line $\mathbb{R}$ and the circle $S^1 = \mathbb{R}/\mathbb{Z}$. The map:

$$p : \mathbb{R} \to S^1, \quad p(t) = e^{2\pi i t},$$

is a covering map. The preimage of any point in S^1 under p is an infinite, discrete set of points in $\mathbb{R}$. Here, $\mathbb{R}$ 'unwraps' the circle into an infinite line.

In this example, $\mathbb{R}$ serves as the universal cover of S^1. The covering map p wraps the real line around the circle infinitely many times, illustrating how a non-simply connected space can be related to a simply connected one.

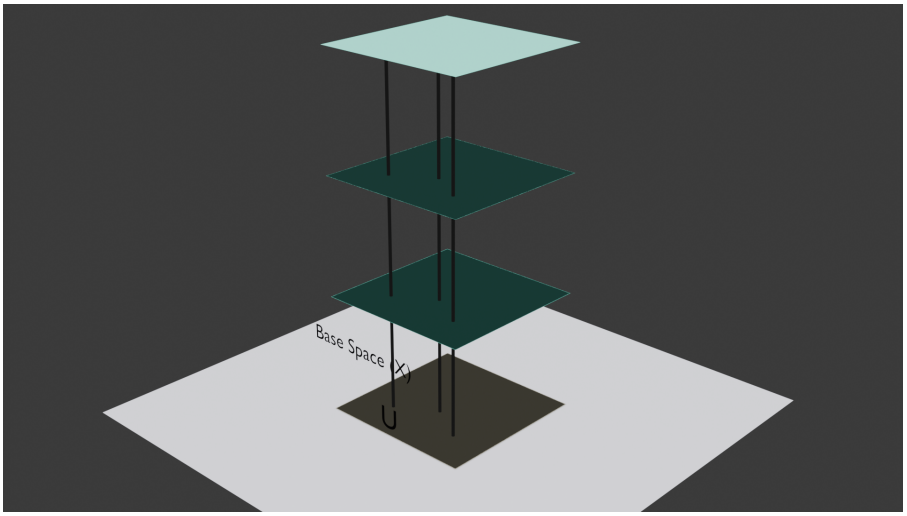

Figure 3: Abstract representation of the covering map, p, with an open neighborhood U in X. The green sheets make up $p^{-1}(U)$, the fibers in black extending down are preimages from each point $p^{-1}(x)$ for $x \in X$.

Example 2.20

For the torus $T^2 = \mathbb{R}^2/\mathbb{Z}^2$, the universal covering space is $\mathbb{R}^2$. The covering map:

$$p : \mathbb{R}^2 \to T^2, \quad p(x, y) = (x \bmod 1, y \bmod 1),$$

unwraps the doubly periodic structure of T^2 into the Euclidean plane.

This example extends the previous one to higher dimensions. The plane $\mathbb{R}^2$ covers the torus by 'tiling' it infinitely in both the x and y directions, allowing us to study the torus using the familiar Euclidean geometry.

The concept of covering spaces becomes even more powerful when applied to manifolds. A natural question arises: can the covering space of a manifold be given a manifold structure itself? The following theorem addresses this.

Theorem 2.21

Let M be an n-manifold, and $(\tilde{M}, p)$ a covering space of M. Then, $\tilde{M}$ can be endowed with the structure of an n-manifold.

Proof. Recall that a smooth n-manifold M has an atlas $\{(U_i, \phi_i)\}$ consisting of coordinate charts where each U_i is an open subset of M and $\phi_i : U_i \to \mathbb{R}^n$ is a homeomorphism.

Since $p : \tilde{M} \to M$ is a covering map, for each chart (U_i, ϕ_i) in M, the preimage $p^{-1}(U_i)$ is a disjoint union of open sets $\{V_{ij}\}$ in $\tilde{M}$, each of which is mapped homeomorphically onto U_i by p. We can define charts on $\tilde{M}$ by composing:

$$\tilde{\phi}_{ij} = \phi_i \circ p|_{V_{ij}} : V_{ij} \to \mathbb{R}^n.$$

These charts cover $\tilde{M}$ and inherit smooth compatibility from those on M because the transition functions on $\tilde{M}$ correspond to those on M. Thus, $\tilde{M}$ acquires the structure of an n-manifold. □

This result ensures that covering spaces of manifolds are themselves manifolds of the same dimension, allowing us to extend manifold concepts and techniques to their covers.

Next, we explore the relationship between a manifold and its universal cover through group actions. Specifically, we want to show that any manifold can be realized as a quotient of its universal cover by a group acting appropriately. Firstly however, we want to see how we can act by groups onto manifolds.

Definition 2.22
A group G is said to be *discrete* if it is a topological group equipped with the discrete topology, meaning that every singleton set $\{g\} \subset G$ is an open set. Equivalently, the elements of G are isolated points, and there is no continuous 'path' between distinct elements of G.

Example 2.23
- The group of integers $\mathbb{Z}$ under addition is a discrete group.
- Discrete subgroups of $SO(n, 1)$, such as those used in hyperbolic geometry.

Definition 2.24
Let G be a group and M a manifold. A *group action* of G on M is a map:

$$\phi : G \times M \to M, \quad \phi(g, x) = g \cdot x,$$

satisfying the following two properties:

1. The identity element $e \in G$ acts trivially on M, i.e., $e \cdot x = x$ for all $x \in M$.
2. For all $g, h \in G$ and $x \in M$,
$$(g \cdot h) \cdot x = g \cdot (h \cdot x).$$

A group action is called:

- *Free* if for all $g \in G \setminus \{e\}$ and $x \in M$, $g \cdot x \neq x$. In other words, no non-identity element of G fixes any point in M.
- *Discontinuous* if for every compact subset $K \subset M$, the set $\{g \in G \mid g \cdot K \cap K \neq \emptyset\}$ is finite. This ensures that the group action avoids accumulation points and that the orbit of any point under G is locally discrete.

Proposition 2.25
Any n-manifold M is the quotient $\tilde{M}/\Gamma$ of its universal cover $\tilde{M}$ by a group Γ acting properly discontinuously and freely on $\tilde{M}$ by orientation-preserving isometries.

Proof. The proof we summarize from [19]. Let Γ denote the group of deck transformations associated with the universal cover $\tilde{M}$. Deck transformations are homeomorphisms $\gamma : \tilde{M} \to \tilde{M}$ satisfying $p \circ \gamma = p$, where $p : \tilde{M} \to M$ is the covering map.

Consider any $\gamma \in \Gamma$ and $z \in \tilde{M}$. The equality $p(\gamma(z)) = p(z)$ indicates that γ permutes the fibers of p. Using the chain rule, we examine the differentials:

$$dp_z = dp_{\gamma(z)} \circ d\gamma_z.$$

Since dp_z is a local isomorphism (as p is a covering map), it follows that $d\gamma_z$ is an isomorphism between the tangent spaces $T_z\tilde{M}$ and $T_{\gamma(z)}\tilde{M}$. Thus, γ is a diffeomorphism.

Moreover, γ preserves the pullback of any Riemannian metric from M to $\tilde{M}$ via p, making γ an isometry. Since $\tilde{M}$ is simply connected, Γ acts freely; that is, if $\gamma(z) = z$ for some $z \in \tilde{M}$, then γ must be the identity.

$$\begin{array}{ccc} \tilde{M} & \xrightarrow{\gamma} & \tilde{M} \\ {\scriptstyle p}\downarrow & \swarrow_{p} & \\ M & & \end{array}$$

To show that Γ acts properly discontinuously, consider any compact subset $K \subset \tilde{M}$. There are only finitely many $\gamma \in \Gamma$ such that $\gamma(K) \cap K \neq \emptyset$, because otherwise, their images under p would accumulate in M, contradicting the local homeomorphism property of p.

Therefore, Γ acts properly discontinuously and freely by orientation-preserving isometries on $\tilde{M}$. The quotient $\tilde{M}/\Gamma$ inherits the manifold structure and is homeomorphic to M via the covering map p. Hence, $M \cong \tilde{M}/\Gamma$.

2.3 Hyperbolic Space

It is important firstly to provide various models with which we will be working. In this section, we can identify all hyperbolic manifolds via H^n, with $n = 3$, since all the respective models are in fact isometrically diffeomorphic to one another, giving translations from model to model as we wish. We will follow the discussion in [20] for descriptions of the models.

Definition 2.26

In the hyperboloid model, we view the space as a hypersurface,

$$H^n = \{x \in \mathbb{R}^{n+1} | (x^1)^2 + \ldots + (x^n)^2 - (x^{n+1})^2 = -1, x^{n+1} > 0\}. \tag{2.3}$$

For the case $n = 3$, this gives the points in $\mathbb{R}^4$ which satisfy

$$-(x^0)^2 + (x^1)^2 + (x^2)^2 + (x^3)^2 = 1,$$

with a corresponding metric of the form

$$-(dx^0)^2 + (dx^1)^2 + (dx^2)^2 + (dx^3)^2 = ds^2. \tag{2.4}$$

The corresponding isometry group is the group of Lorentz transformations, $SO(3,1) \cong PSL(2,\mathbb{C})$. We can introduce pseudospherical coordinates (ρ, θ, ϕ) via the mapping:

$$\begin{aligned} x^0 &= \cosh\rho, & x^1 &= \sinh\rho\sin\theta\cos\phi, \\ x^2 &= \sinh\rho\sin\theta\sin\phi, & x^3 &= \sinh\rho\cos\theta, \end{aligned} \tag{2.5}$$

with $0 \leq \rho < \infty$, $0 \leq \theta \leq \pi$, $0 \leq \phi \leq 2\pi$. This coordinate shift leaves the metric (2.4) as the following:

$$ds^2 = d\rho^2 + \sinh^2(\rho)(d\theta^2 + \sin^2(\theta)d\phi^2). \tag{2.6}$$

Definition 2.27

The Poincaré ball model results from transforming the pseudospherical coordinates (2.5) into an open ball, $H^3 = \{x \in \mathbb{R}^3 | (x^0)^2 + (x^1)^2 + (x^2)^2 < 1\}$. This can be achieved via the transformation:

$$x^0 = \tanh\frac{\rho}{2}\sin\theta\cos\phi, \quad x^1 = \tanh\frac{\rho}{2}\sin\theta\sin\phi, \quad x^2 = \tanh\frac{\rho}{2}\cos\theta.$$

The metric in this model becomes

$$ds^2 = 4\frac{(dx^0)^2 + (dx^1)^2 + (dx^2)^2}{(1 - (x^0)^2 + (x^1)^2 + (x^2)^2)}. \tag{2.7}$$

The hyperbolic distance between two points $\boldsymbol{x}$ and $\boldsymbol{x}'$ in the ball model is computed using:

$$d(\boldsymbol{x}, \boldsymbol{x}') = \operatorname{arccosh}\left(1 + \frac{2|\boldsymbol{x} - \boldsymbol{x}'|^2}{(1 - |\boldsymbol{x}|^2)(1 - |\boldsymbol{x}'|^2)}\right). \tag{2.8}$$

Definition 2.28

In the Klein model, starting from the pseudospherical coordinates (2.5), we map

$$x^1 = \tanh\rho\sin\theta\cos\phi, \quad x^2 = \tanh\rho\sin\theta\sin\phi, \quad x^3 = \tanh\rho\cos\theta. \tag{2.9}$$

This projects the hyperboloid into the sphere $(1, x^0, x^1, x^2)$ along the lines from the origin. The geodesic distance between two points $\tilde{\mathbf{x}}, \tilde{\mathbf{x}}'$ in this model is given by:

$$\cosh[d(\mathbf{x}, \mathbf{x}')] = \frac{1 - \tilde{\mathbf{x}} \cdot \tilde{\mathbf{x}}'}{\sqrt{(1 - |\tilde{\mathbf{x}}|^2)(1 - |\tilde{\mathbf{x}}'|^2)}}. \tag{2.10}$$

These models are what we will make use of during our computations. Now let us take a deeper look at how our specific cases of hyperbolic manifolds tie in with the concepts of an isometry group, which we had defined previously. We will follow the discussion presented in [21] for the most part.

In the hyperboloid model, isometries correspond to linear transformations of the ambient Minkowski space $\mathbb{R}^{n+1}$ that preserve the hyperboloid H^n and the Minkowski metric:

$$g(x, y) = -x^0y^0 + x^1y^1 + \cdots + x^ny^n.$$

These transformations form the Lorentz group $O(n, 1)$, consisting of all linear maps $L : \mathbb{R}^{n+1} \to \mathbb{R}^{n+1}$ satisfying

$$\langle Lx, Ly\rangle = \langle x, y\rangle.$$

However, not all elements of $O(n, 1)$ preserve the orientation and the time direction (i.e., the condition $x^{n+1} > 0$ in (2.3)). The subgroup of $O(n, 1)$ that preserves both orientation and the upper sheet of the hyperboloid is the *proper Lorentz group*, denoted $SO^+(n, 1)$.

For our case with $n = 3$, the isometry group of hyperbolic 3-space H^3 is thus identified with $SO^+(3, 1)$. These transformations preserve the metric given in (2.4). To better understand how isometries act in this setting, let us consider the following example.

Example 2.29

In the hyperboloid model, isometries are represented by Lorentz transformations. For a point $x \in H^3$, an isometry can be expressed as $x \mapsto Lx$, where $L \in SO^+(3,1)$. The Lorentz transformation L preserves the Minkowski inner product, ensuring that the transformed point Lx remains on the hyperboloid:

$$\langle Lx, Lx\rangle = \langle x, x\rangle = -1.$$

For example, consider a boost in the x^1 direction, represented by:

$$L = \begin{pmatrix} \cosh(\eta) & \sinh(\eta) & 0 & 0 \\ \sinh(\eta) & \cosh(\eta) & 0 & 0 \\ 0 & 0 & 1 & 0 \\ 0 & 0 & 0 & 1 \end{pmatrix},$$

where η is a parameter describing the amount of the boost. This transformation translates points along a geodesic in H^3.

Returning to the hyperboloid model, the connection between $SO^+(3,1)$ and $PSL(2,\mathbb{C})$ allows us to express isometries in terms of matrix actions. Specifically, the group $SL(2,\mathbb{C})$ acts on Minkowski space by conjugation:

$$X \mapsto AXA^\dagger,$$

where X is the Hermitian matrix associated with a point in $\mathbb{R}^{3,1}$, and $A \in SL(2,\mathbb{C})$. Since $\det(A) = 1$, this action preserves the determinant of X, which corresponds to the Minkowski norm.

The kernel of this action consists of $\{\pm I\}$, leading to the isomorphism:

$$SO^+(3,1) \cong PSL(2,\mathbb{C}).$$

In summary, isometries in hyperbolic space H^3 preserve the underlying geometry of the models described earlier, and their algebraic structure is captured by the isometry group $SO^+(3,1)$, which is isomorphic to $PSL(2,\mathbb{C})$. These isometries form the backbone of hyperbolic geometry, enabling the exploration of hyperbolic manifolds and their rich properties.

2.4 Hyperbolic Manifolds

We present some results on hyperbolic manifolds necessary to the discussion we wish to have further on. In particular, we wish to motivate the idea of the 'tesselation' of the universal covering space of any manifold we choose via copies of the compact space $\tilde{M}/\Gamma$.

Proposition 2.30

If M is a compact hyperbolic n-manifold, then the universal cover of M is the hyperbolic space H^n.

Proof. By the Cartan-Hadamard Theorem [22], we know that every simply-connected, complete hyperbolic n-manifold is isometric to H^n. Furthermore, by definition, any closed, compact

manifold is necessarily complete, thereby making any covering space imposed on it also complete. Therefore, by Theorem 2.21, the universal cover of M is by definition a simply connected covering space, $\tilde{M}$, which is complete, and unto which we may endow a hyperbolic manifold structure, such that $\tilde{M} \cong H^n$.

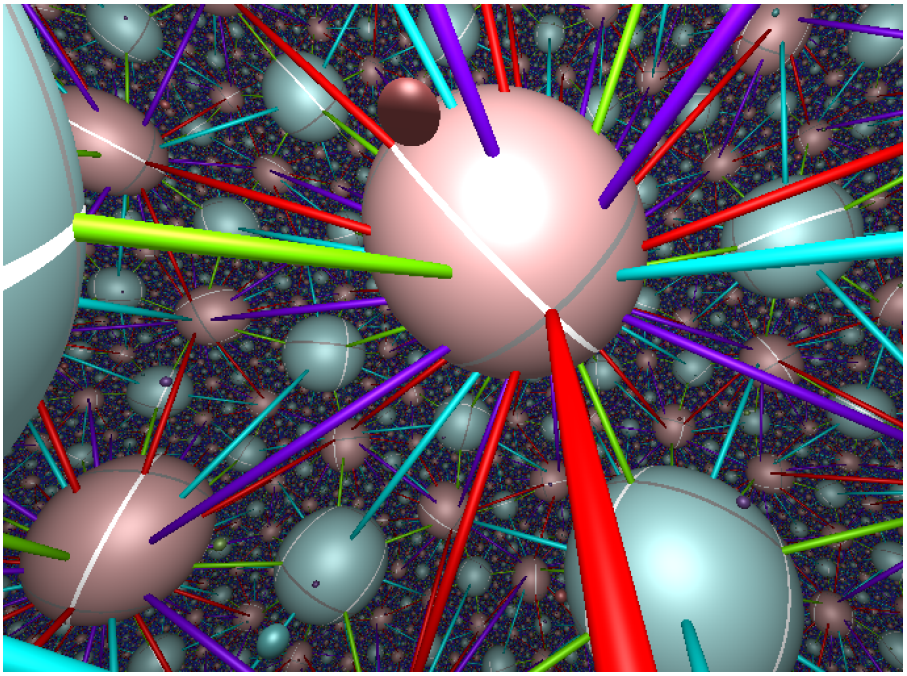

Figure 4: A view from inside of the hyperbolic manifold $m125$, computed with *SnapPea* [23]. The solid colored lines outline the shape of the fundamental domain, the vertices are the spherical connection points.

Definition 2.31

A *fundamental domain* for the action of a group Γ on a space X is a subset $D \subset X$ such that:

1. The images of D under Γ cover X:
$$X = \bigcup_{\gamma \in \Gamma} \gamma D.$$
2. The interiors of the images are pairwise disjoint:
$$\gamma D^\circ \cap \gamma' D^\circ = \varnothing \quad \text{for all } \gamma, \gamma' \in \Gamma, \gamma \neq \gamma',$$
where D° denotes the interior of D.

Definition 2.32

Let M be a manifold with a metric d, and let Γ be a discrete group of isometries acting properly discontinuously on M. Fix a base point $p \in M$. The *Dirichlet domain* $D(p)$ of Γ with respect to p is a *fundamental domain* for the action of Γ on M defined as:
$$D(p) = \{x \in M \mid d(x,p) \leq d(x,\gamma p),\ \forall \gamma \in \Gamma,\ \gamma \neq \mathrm{id}\}.$$

In this context:

1. $D(p)$ satisfies the properties of a fundamental domain:

   (a) The images of $D(p)$ under Γ cover M:

   $$M = \bigcup_{\gamma \in \Gamma} \gamma D(p).$$

   (b) The interiors of these images are pairwise disjoint:

   $$\gamma D(p)^\circ \cap \gamma' D(p)^\circ = \varnothing \quad \text{for all } \gamma, \gamma' \in \Gamma,\ \gamma \neq \gamma'.$$

2. $D(p)$ is bounded by the *perpendicular bisectors* (or hyperplanes) between p and its images γp under the action of Γ. These boundaries ensure that each point $x \in D(p)$ is closer to p than to any other γp, where $\gamma \neq \mathrm{id}$.

Thus, $D(p)$ can be interpreted as a specific construction of a fundamental domain using the distance metric d and the fixed base point p.

Example 2.33

Consider the Euclidean plane $\mathbb{R}^2$ with the group Γ of translations by integer multiples of 1 along both axes:

$$\Gamma = \{(x, y) \mapsto (x + m, y + n) \mid m, n \in \mathbb{Z}\}.$$

Let $p = (0, 0)$. The Dirichlet domain $D(p)$ is the square:

$$D(p) = \{(x, y) \in \mathbb{R}^2 \mid -\frac{1}{2} \leq x \leq \frac{1}{2}, -\frac{1}{2} \leq y \leq \frac{1}{2}\}.$$

This square tiles the entire plane under the action of Γ, with edges identified.

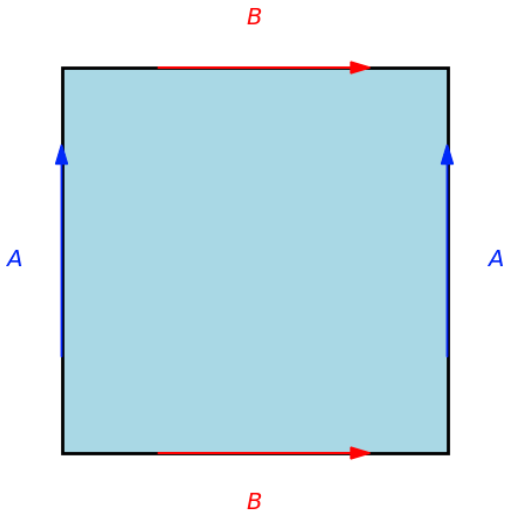

Figure 5: Dirichlet domain, identifying the edges with red and blue with A and B lettering to indicate gluing. This also forms a torus, T, if we actually do the gluing. Using the Dirichlet domain, we can tile the entirety of $\mathbb{R}^2$, as should be visually clear.

Having established that any compact hyperbolic n-manifold M can be expressed as the quotient H^n/Γ, where Γ is a discrete group of isometries acting properly discontinuously on H^n, we now explore how the universal cover H^n can be partitioned into copies of a fundamental domain associated with M. This partitioning, or tiling, provides deep insight into the geometric structure of M and the action of Γ.

In the context of hyperbolic manifolds, the fundamental domain D serves as a 'tile' that, when acted upon by the elements of Γ, fills the entire hyperbolic space H^n without overlaps in their interiors. The manifold M itself can be viewed as the fundamental domain D with appropriate identifications on its boundary according to the action of Γ.

Example 2.34 (Tiling in H^2)
Consider the hyperbolic plane H^2 represented in the Poincaré disk model. The modular group $\Gamma = PSL(2, \mathbb{Z})$ acts on H^2 by Möbius transformations, preserving the hyperbolic structure. A fundamental domain for this action is a region in the Poincaré disk that tiles the entire hyperbolic plane under the group action.

In the Poincaré disk model, the geodesics are represented by circular arcs orthogonal to the boundary of the disk. The tiling in the figure consists of infinitely many curved triangles (ideal triangles) that fit together perfectly without gaps or overlaps. These triangles are images of the fundamental domain under the action of Γ. Each arc in the figure corresponds to a hyperbolic geodesic, and the boundaries of the triangles are formed by these geodesics.

This tiling serves as a visualization of the structure of H^2 under the modular group, with the circular boundary of the disk representing the infinity of hyperbolic space.

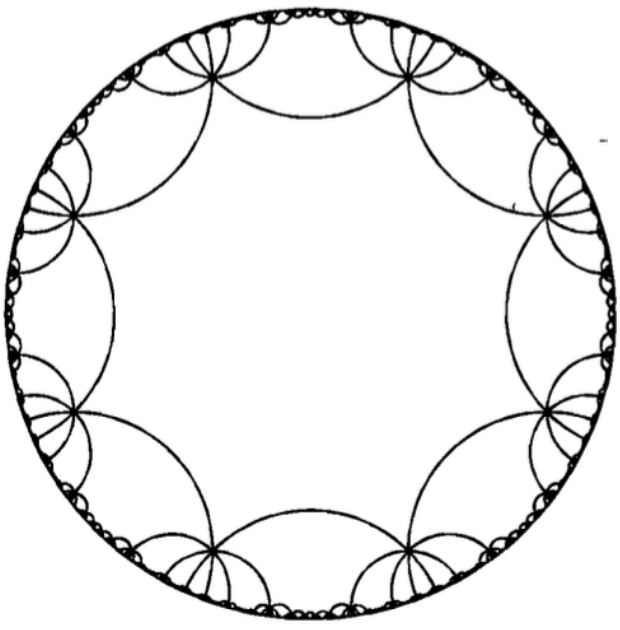

Figure 6: Tiling of the Poincare Disk by octagons [24]

In higher dimensions, similar constructions apply. For a compact hyperbolic 3-manifold M, its

universal cover H^3 can be tiled by copies of a fundamental domain associated with M. Each copy corresponds to an element of the deck transformation group Γ.

When attempting to visualize a hyperbolic manifold $M = H^n/\Gamma$, one strategy is to consider the fundamental domain D within H^n and understand how Γ acts to replicate D throughout the space. Each image γD for $\gamma \in \Gamma$ can be thought of as a 'ghost' of the original domain D. This terminology arises from the idea that these images are not part of the manifold M itself but are artifacts of viewing M within its universal cover H^n.

Example 2.35

Consider the Poincaré dodecahedral space. Its fundamental domain can be represented by a regular dodecahedron in H^3, where opposite faces are identified after a rotation of $\frac{\pi}{5}$. The group Γ consists of isometries corresponding to these face identifications.

In the universal cover H^3, the manifold's structure is revealed through an infinite tiling by copies of this dodecahedral fundamental domain. Each copy is related to the others by elements of Γ, and collectively, they fill H^3 in a regular pattern. The 'ghosts' are these other copies of the fundamental domain, which are not directly part of the manifold but represent how the manifold's local geometry extends throughout hyperbolic space.

Mathematically, the tiling by fundamental domains illustrates how the action of Γ partitions H^n into equivalent regions. Each point in H^n can be mapped back to the fundamental domain D via some $\gamma^{-1} \in \Gamma$, ensuring that the manifold M inherits its geometry from the universal cover.
The identification of boundary points of D under Γ defines the topology of M. For instance, if two faces of D are identified via an isometry $\gamma \in \Gamma$, then in M, these faces are glued togeether, and paths crossing from one face to the other are continuous within the manifold.

The term 'ghosts' captures the notion that the other copies of D in H^n are like spectral images—visible in the universal cover but not present in the manifold M itself. When considering physical models or simulations, observers within M might interpret light paths that traverse the manifold's topology and re-enter through another identified face as coming from a 'ghost' image.

3 Hearing the Shape of the Universe

The mathematical framework we developed here in the previous sections provides the tools necessary to model and analyze these aspects of the universe relating to the global topology we want to observe by examining the anistropies in the Cosmic Microwave Background (CMB) radiation. Observations of the CMB reveal slight anisotropies, or fluctuations in temperature, which are believed to be the result of quantum fluctuations amplified during cosmic inflation. The size of these temperature anisotropies are quite small, $\delta T/T \approx \pm 10^{-5}$.

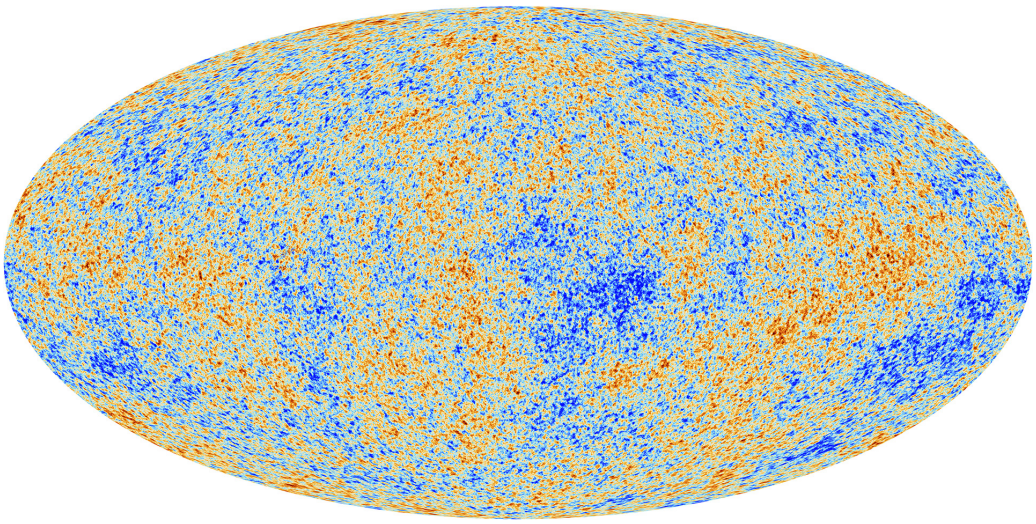

Figure 7: The joint observations of the CMB anisotropies by the European Space Agency (ESA) and the Planck mission reveal minute temperature fluctuations represented by various colors [25]. These variations correspond to regions of slightly different densities, which serve as the seeds for all subsequent structures in the universe, including galaxies and stars as we observe them today.

The topology of the universe can leave imprints on these CMB fluctuations. In a universe with a non-trivial topology, such as one modeled by a compact hyperbolic manifold, the allowed modes of vibration (eigenmodes) are quantized due to the finite extent of space. This quantization affects the spectrum of temperature fluctuations observed in the CMB.

By solving the Laplace equation (3.4) on a compact hyperbolic manifold, we can determine the eigenvalues q^2 corresponding to the vibrational modes of the universe. These eigenvalues influence the power spectrum of the CMB anisotropies. If the universe has a compact hyperbolic topology, there may be a suppression of fluctuations at large scales, which could provide an explanation for certain anomalies observed in the CMB data [26].

Furthermore, the method of images, or the 'method of ghosts' allows us to construct eigenfunctions on the manifold by considering contributions from multiple copies (images) of a point under the action of the covering group Γ . This approach is analogous to considering multiple paths that light could take in a multiply connected space, potentially leading to observable effects such as repeating patterns in the sky or multiple images of distant objects.

Mathematically, the goal would be to explain temperature anisotropies in the CMB using the

eigenvalues and eigenfunctions of the Laplace operator on spaces with the geometry we wish to probe. In particular, given a set of eigenvalues, $\{q_n\}$, we can obtain corresponding eigenfunctions, Ψ_{q_n}. Then, the temperature fluctuations in the CMB we can treat as a function $\delta T(x)$. To provide some context, we guess that the CMB anisotropies here originate from metric and density pertubations in the early universe, the imprint of which we want to search for in the photon field [13]. So we treat $\delta T(x)$ as a function on a spatial hypersurface of constant cosmic time, which we can expand mathematically using our set of eigenvalues and eigenfunctions

$$\delta T(x) = \sum_n a_n \Psi_{q_n} \tag{3.1}$$

then the angular power spectrum of the CMB, defined by

$$C_\ell = \frac{1}{2\ell+1} \sum_{m=-\ell}^{\ell} \langle a_{\ell m} a^*_{\ell m} \rangle, \tag{3.2}$$

is directly influenced by the set of eigenvalues $\{q_n\}$ and eigenfunctions $\{\Psi_{q_n}\}$ [13].

In a compact hyperbolic universe, the discrete and quantized nature of q_n alters the distribution of modes available, potentially suppressing large-scale power. Such suppression at low ℓ could manifest as observable deviations from the predictions of infinite, simply connected models. Thus, by measuring and analyzing C_ℓ in the CMB data, we can attempt to "hear" the global shape of the universe encoded in the eigenvalue spectrum of its underlying geometry.

3.1 Method of Ghosts

The *method of ghosts* is the primary tool which we want to make use of in the context of our algortihm, we provide some more detail as to the specifics here. We had touched a bit on conceptual aspects when introducing the fundamental and Dirichlet domains, and tilings of the space. The Dirichlet domain corresponding to the specific compact manifold over which we are working is in a sense a 'folded' version of the entire manifold. Due to the difficulties of actually visualizing compact hyperbolic manifolds, the best way with which we can do this is via the Dirichlet domain.

When picking points inside the domain, and then transforming them via some $\gamma \in \Gamma$, so, essentially looking at the image $\gamma(D)$, we obtain the 'ghosts' of the original image, as copies of the original. Much like how you would see copies of yourself in a hall of mirrors. So this in the sense that we send all our points into the covering space, from our domain. We can also do the opposite, and fold back up the manifold to return back to the original domain we started with. Mathematically, we formulate this in terms of the invariance

$$\Psi(x) = \Psi(\gamma x) \tag{3.3}$$

for any smooth function Ψ on the manifold and $\gamma \in \Gamma$.

Theorem 3.1

Let $\Sigma = H^3/\Gamma$ be a compact hyperbolic 3-manifold, where $\Gamma \subset PSL(2,\mathbb{C}) \cong SO(3,1)$ is a discrete, torsion-free subgroup acting freely and discontinuously on H^3. Denote the Laplace operator on Σ by Δ_Σ and on H^3 by Δ_{H^3}. For any eigenfunction $\Psi : \Sigma \to \mathbb{R}$ of Δ_Σ satisfying

$$\Delta_\Sigma \Psi + q^2 \Psi = 0,$$

there exists a corresponding eigenfunction $\tilde{\Psi} : H^3 \to \mathbb{R}$ of Δ_{H^3}, satisfying

$$\Delta_{H^3}\tilde{\Psi} + q^2\tilde{\Psi} = 0,$$

such that $\tilde{\Psi}$ is Γ-invariant, i.e.,

$$\tilde{\Psi}(\gamma x) = \tilde{\Psi}(x), \quad \forall \gamma \in \Gamma,\, x \in H^3.$$

Proof. Let $\pi : H^3 \to \Sigma$ be the natural projection induced by the quotient structure $\Sigma = H^3/\Gamma$, which identifies points related by the action of Γ. Since π is a local isometry, the Laplace operators on Σ and H^3 are related such that, for any smooth function $f : \Sigma \to \mathbb{R}$, its pullback $\tilde{f} = f \circ \pi$ satisfies

$$\Delta_{H^3}\tilde{f}(x) = (\Delta_\Sigma f)(\pi(x)).$$

Now, consider an eigenfunction $\Psi : \Sigma \to \mathbb{R}$ of Δ_Σ with eigenvalue $-q^2$, i.e., $\Delta_\Sigma\Psi + q^2\Psi = 0$. Define the pullback function $\tilde{\Psi} : H^3 \to \mathbb{R}$ by

$$\tilde{\Psi}(x) = \Psi(\pi(x)).$$

By the compatibility of the Laplacian under pullback, we have

$$\Delta_{H^3}\tilde{\Psi}(x) = (\Delta_\Sigma\Psi)(\pi(x)) = -q^2\Psi(\pi(x)) = -q^2\tilde{\Psi}(x),$$

showing that $\tilde{\Psi}$ is an eigenfunction of Δ_{H^3} with eigenvalue $-q^2$.
To establish Γ-invariance, let $\gamma \in \Gamma$. Then, for any $x \in H^3$,

$$\tilde{\Psi}(\gamma x) = \Psi(\pi(\gamma x)).$$

Since $\pi(\gamma x) = \pi(x)$ by the definition of the quotient space, it follows that

$$\tilde{\Psi}(\gamma x) = \Psi(\pi(x)) = \tilde{\Psi}(x).$$

Thus, $\tilde{\Psi}$ is invariant under the action of Γ. □

Furthermore, the Γ-invariance of $\tilde{\Psi}$ implies that it can be expressed as a linear combination of eigenfunctions of Δ_{H^3} that respect the periodic boundary conditions imposed by Γ. Specifically, we can write

$$\Psi(x) = \sum_{(\ell,m)} a_{\ell m} Q_{q\ell m}(x),$$

where $Q_{q\ell m}$ are eigenfunctions of Δ_{H^3}, and the coefficients $a_{\ell m}$ are determined by the symmetry constraints.

Finally, the compatibility condition $\tilde{\Psi}(\gamma x) = \tilde{\Psi}(x)$ for all $\gamma \in \Gamma$ restricts the eigenvalues q^2 to those in the spectrum of Δ_Σ, ensuring a one-to-one correspondence between the eigenfunctions on Σ and Γ-invariant eigenfunctions on H^3.

3.2 Outline of the problem

In order to achieve the goal of simulating the early universe, and in particular achieving the kind of fluctuations that are visible in the CMB projections, we need to construct the vibrational modes assumed to be behind them. If it is true that the particular topology of the universe does indeed effect these deviations from homogeneity we need a way to connect the two. Let Σ be a compact hyperbolic n-manifold. By virtue of Theorem 2.21, we know that any universal cover of Σ can be endowed with the structure of a hyperbolic manifold, and moreover we know that in this case, the universal cover is in fact H^n, by Proposition 2.30. Furthermore, Proposition 2.25 tells us that in fact $\Sigma \cong H^n/\Gamma$, as a compact manifold, with $\Gamma \subset PSL(2,\mathbb{C}) \cong SO(3,1)$ being a discrete subgroup describing the isometries on Σ acting freely and discontinuously on it. The Laplace equation, we write as

$$(\Delta + q^2)\Psi = 0 \tag{3.4}$$

with Δ as the Laplace operator and q^2 an eigenvalue of Δ. From the discussion of hyperbolic spaces, we borrow the hyperboloid model (2.3), and apply the pseudospherical change of coordinates (2.5), giving us coordinates on the hyperbolic manifold as $(x^i) = (x^0, x^1, x^2) = (\rho, \theta, \phi) \in H^3$.

The influence of the topology as mentioned earlier now truly comes into view in the expression that will be obtained for the Laplacian on these coordinates. To derive the Laplacian in the coordinates (ρ, θ, ϕ) for the hyperbolic manifold H^3, we start with the general, coordinate-free definition of the Laplacian. Let (M, g) be a Riemannian manifold with metric g. The Laplace-Beltrami operator Δ applied to a smooth function $f : M \to \mathbb{R}$ is defined as:

$$\Delta f = \operatorname{div}(\operatorname{grad}(f)),$$

Without going too much detail, taking a chart on M and choosing some local coordinates (x^i), it is possible to get expressions for both the divergence and gradient operators. Thus in local coordinates (x^i) with the metric tensor (2.6) components g_{ij}, the Laplacian is expressed as:

$$\Delta f = \frac{1}{\sqrt{|g|}} \frac{\partial}{\partial x^i} \left(\sqrt{|g|} g^{ij} \frac{\partial f}{\partial x^j} \right), \tag{3.5}$$

where $g = \det(g_{ij})$ is the determinant of the metric tensor and g^{ij} are the components of the inverse metric. In the pseudospherical coordinates, we recall that the hyperbolic metric g takes the form from (2.6):

$$ds^2 = d\rho^2 + \sinh^2(\rho) \left(d\theta^2 + \sin^2(\theta)\, d\phi^2 \right).$$

For easy of computation, we introduce the substitution $r = \sinh(\rho)$. The inverse metric components g^{ij} are:

$$g^{rr} = 1 + r^2, \quad g^{\theta\theta} = \frac{1}{r^2}, \quad g^{\phi\phi} = \frac{1}{r^2 \sin^2(\theta)}.$$

Then, the determinant of the metric tensor in these coordinates is simply $|g| = r^4 \sin^2(\theta)$. Combining all the expressions we have obtained, we can obtain the expression of the Laplacian on the local coordinates on the universal covering space of H^3 as

$$\Delta = \frac{1}{\sqrt{|g|}} \frac{\partial}{\partial x^i} \left(\sqrt{|g|} g^{ij} \frac{\partial}{\partial x^j} \right)$$

$$\overset{(*)}{=} \frac{1}{\sinh^2(\rho)}\left(\partial_\rho(\sinh^2(\rho)\partial_\rho) + \frac{1}{\sin(\theta)}\partial_\theta(\sin(\theta)\partial_\theta) + \frac{1}{\sin^2(\theta)}\partial_\phi^2\right)$$

wherein $(*)$ we reverted the substitution. We can apply Δ on smooth functions living in H^3, $\Psi : \Sigma \to \mathbb{R}$, such that[3]

$$(\Delta + q^2)\Psi = \Delta\Psi + q^2\Psi = \left(\frac{1}{\sinh^2(\rho)}(\Delta^\rho\Psi + \Delta^{\theta,\phi}\Psi) + q^2\Psi\right) = 0. \tag{3.6}$$

This means in particular if we assume that $Q_{qlm}(x) = Q_{qlm}(\rho,\theta,\phi) = X_q^l(\rho)\cdot Y_{lm}(\theta,\phi)$, where $X_q^l(\rho)$ are the hyperspherical bessel functions, and $Y_{lm}(\theta,\phi)$ are the standard spherical harmonics, then we can indeed solve (3.6) by using the invariance property of Ψ under Γ. Note that for convenience we also split the inside of the parantheses into the radial and harmonic parts for ease of computation/ Continuing from (3.6), using our ansatz, we get seperate differential equations, the details of which can be found in the appendix. An important note to make also here will be that from now instead of using the eigenvalue q as a sub-index, we will want to make use of a related parameter, the wave number, k, where

$$k^2 = q^2 - 1 \tag{3.7}$$

since indeed this will be the parameter over which we will be iterating for the rest of our method.

What is needed for our purposes are the expressions of the two sets of functions, the first of which, the hyperspherical bessel functions being given by

$$X_k^l(\rho) = \sqrt{\frac{N_k^l}{\sinh(\rho)}}\cdot P^{-1/2-l}_{-1/2+ik}(\cosh\rho) \tag{3.8}$$

with $N_k^l = \prod_{0\le n\le l}(k^2+n^2)$. The spherical harmonics are given by

$$Y_{lm}(\theta,\phi) = \left(\frac{(2l+1)(l-m)!}{4\pi(l+m)!}\right)^{1/2} P_l^m(\cos\theta)e^{im\phi}. \tag{3.9}$$

To continue from here, we make use of the previous mathematical tool in the method of ghosts analysis. We take as a starting points functions Ψ of the form

$$\Psi(g_\alpha p_i) - \Psi(g_\beta p_i) = 0 \tag{3.10}$$

such that we can construct a system of equations of the form[4]

$$\begin{aligned}\Psi(g_\alpha p_i) - \Psi(g_\beta p_i) &= \sum_{l\ge0}\sum_{|m|\le l} a_{lm}Q_{lm}(g_\alpha p_i) - \sum_{l\ge0}\sum_{|m|\le l} a_{lm}Q_{lm}(g_\beta p_j)\\ &= \sum_{l\ge0}\sum_{|m|\le l}(Q(g_\alpha p_i) - Q(g_\beta p_i))a_{lm}\\ &= A\cdot a\end{aligned}$$

[3] We split the radial and spherical portions of the operator here, nothing more.

[4] There is an implicit dependence on the wavenumber parameter, k, here.

where in the end we simply arrive at a matrix equation we need to solve. We have that $A \in \mathbb{R}^{M\times N}$ and $a \in \mathbb{R}^{N\times 1}$. In the first line of the difference of Ψ's, we choose $\alpha, \beta \in \{1, 2, \ldots, |\Gamma|\}$, and $\alpha \neq \beta$ such that g_α and g_β are the face-pairing generators of Γ. Moreover we choose points $p_i \in D_\Sigma$ in the Dirichlet domain of Σ, such that when acted on by the face-pairing generators, they are sent out into the universal cover, producing a number of images, n_i. We specify this number of images produced since in practice we choose to constrain the number of images we collect for each point up to a certain maximum distance inside the covering space.

In total, counting the number of images for each point, n_i, and choosing a total of d many points in the domain itself, the number of equations in the form of (3.10) we can construct is a total of $n_i(n_i-1)/2$ for each point p_i. Such that the matrix we construct is of the form

$$\begin{bmatrix} (Q_{00}(g_1p_1) - Q_{00}(g_2p_1)) & \cdots & (Q_{LL}(g_1p_1) - Q_{LL}(g_2p_1)) \\ \vdots & \ddots & \vdots \\ (Q_{00}(g_\alpha p_d) - Q_{00}(g_\beta p_d)) & \cdots & (Q_{LL}(g_\alpha p_d) - Q_{LL}(g_\beta p_d)) \end{bmatrix} \begin{bmatrix} a_{00} \\ \vdots \\ a_{LL} \end{bmatrix} = \begin{bmatrix} 0 \\ \vdots \\ 0 \end{bmatrix}. \tag{3.11}$$

The number of rows of the matrix is as the sum

$$M = \sum_{i=1}^{d} \frac{n_i(n_i-1)}{2} \tag{3.12}$$

and the number of columns of the matrix, N, is as

$$N = \sum_{l\geq 0} \sum_{|m|\leq l} 1 = (L+1)^2. \tag{3.13}$$

As we go down the rows, we simply change the pairs of generators we apply to each point till we reach the $n_i(n_i-1)/2$ number of rows possible for each points, and then repeat the process. In (3.11), each row represents a concatenated version of the $n_i(n_i-1)/2$ number of rows we would have for each point.

Since we wish to solve the system $A \cdot a = 0$, we want to look at the matrix A for different choices of M and N. We can quickly see from results in linear algebra that a non-trivial solution exists only when $\det(A) = 0$. When k is not an eigenvalue, the rows of A become linearly independent, giving the matrix full rank, and hence only corresponding to the trivial solution. However, when k is an eigenvalue, then there exist non-trivial eigenmodes on the covering space which would satisfy (3.6), and hence make it such that the matrix would have rows which are linearly dependent. Thus, if $M = N - 1$, then the nullspace of the matrix has only a single dimensional null-space, allowing the system to have a solution for any choice of k. Moreover, when $M > N$, we have an over-determined system, and a solution only when k corresponds to an eigenvalue.

To solve the over-determined system of equations, we choose to use the method of the singular value decomposition (SVD). Using the SVD, we can obtain the eigenmodes which would form a basis for the nullspace of A. The SVD returns A as a product of matrices $U \in \mathbb{R}^{M\times N}$ unitary, $D \in \mathbb{R}^{N\times N}$ diagonal, and $V \in \mathbb{R}^{N\times N}$ unitary, as

$$A = UDV^T. \tag{3.14}$$

The columns of U form an orthonormal basis which spans the range of A, and the columns of V which correspond to the singular values, diagonal entries in D form the basis for the nullspace of A. Numerically, we can only obtain values which are close to 0 but not exactly 0, by choosing for the solution vector, the columns of V which correspond to the smallest singular values in D. In particular, we compute the quantity

$$\chi^2 = |A \cdot a|^2 \tag{3.15}$$

while iterating over the parameter k. The SVD minimizes this this χ^2 over the range of k, revealing along the way the eigenvalues as minima in $\chi^2(k)$. These minima are revealed since, essentially, we are measuring the solvability of the system $A \cdot a$, the smaller the singular values returned by the SVD, the more likely it is that we have found an eigenvalue. Ideally, the smallest singular values would drop to 0, exactly revealing the eigenvalues, however numerically this won't be the case since we are working with matrices of finite size. Eigenvalues with multiplicity greater than 1 will have multiple solution vectors attached to them, in that the SVD will return solution vectors a matching the multiplicity of the eigenvalue.

4 Implementation

Given the description of the method, it is also necessary to talk about the specific parameters varying and changing and being selected throughout. In particular, we need to make choices for the parameters of L, $\rho_{\max}$, and $c = M/N$.

The parameter most important here is the degree of over-constraint, c, which is chosen to be the ratio of the rows to columns within the matrix A. The method, as far as we know, fails for a wrong choice of c. Moreover, [1] furthermore makes a choice of some $l_{\max}$ parameter in order to determine $\rho_{\max}$ but however fails to explain the exact details, and the construction which they provide simply breaks down in actual implementation. In particular, the method by which the tiling radius, $\rho_{\max}$ is determined in the paper does not produce sensible results. In [1], an approximation of the hyperspherical bessel functions is used to describe the general behavior of the function

$$X_k^l(\rho) \approx \begin{cases} 0 & \rho < \rho_0 \\ \frac{\cos(k\rho+\phi_0)}{\sinh(\rho)} & \rho > \rho_0 \end{cases} \tag{4.1}$$

which is then used to solve the following equation for the first ρ which satisfies it

$$X_k^l(\rho) \cdot \sinh(\rho) = 0.25. \tag{4.2}$$

The paper provides no information on the constants ρ_0 and ϕ_0, apart from that they depend on k on l. Luckily, [27] provides an expression for ρ_0, which, after some computation gives ϕ_0 as a multiple of ρ_0 as

$$\rho_0 = \operatorname{arcsinh}\left(\frac{\sqrt{l(l+1)}}{k}\right), \quad \phi_0 = -k\rho_0. \tag{4.3}$$

No context is provided for (4.2) and although the approximation (4.1) does provide a sensible approximation, the description of choosing the $l_{\max}$ and $l_{\min}$ and solving (4.2) yields a higher value of $\rho_{\max}$ for the $l_{\min}$ value than $l_{\max}$. Nonetheless, we borrow certain choices for parameters L and k, where k is again the wavenumber parameter in (3.7). The choices we followed from [1] are the following

$$L = 10 + [k] \tag{4.4}$$

$$c = 10 + [100/k]. \tag{4.5}$$

Such that, for each value of k for which we iterate over, we obtain a new c and L, which determine the size of the matrix, i.e. linear system, which we are solving. Note also the brackets around the expressions containing k serve to round the expression inside them to the closest integer.

Furthermore, we also included the added parameter $\rho_{\min}$ to determine an inner-cut off radius, mimicking the choices made in the description of the parameter choices in [1].

4.1 Domain Construction and Point Selection

In order to find points and select them inside the Dirichlet domain, we needed to construct the domain itself. We did this via both the definition of the domain in (2.32), and also by asking

SnapPea [23] for information regarding the structure of the domain. In particular, we can construct the domain in Klein hyperbolic coordinates, using the data available on the specific quantities which define the polyhedron. Since lines in Klein space are as straight as standard Euclidean lines, the construction of the polyhedron relies only on information regarding the locations of the vertices, edges connecting them, and the faces. As two chosen examples, we plotted the manifolds $\Sigma = m188(-1,1)$ and $m003(-3,1)$. We had to then write code which

(a) Domain $m003(-3,1)$ (b) Domain $m188(-1,1)$

Figure 8: Example domains with a point inside on display.

would return, given a specific manifold, a number of randomly chosen points inside the domains, along with what the images of the points under transformations by the face-pairing generators would be. We found these images by again calling SnapPea for the generators, which would be returned in their representation as matrices in $SO(3,1)$. We plotted points found inside the domains and moreover the images of the domain, 'tiling' the hyperbolic space, clearly visible, Indeed what is clear to see also in the picture is the fact that the images under the face-pairing generators indeed connect the various tiles at the faces which they originate from.

The code which computes all of this has the geometry functions imbedded, such that we return the coordinates of the sampled points in pseudospherical coordinates.

4.2 Coding and Optimization

In order to implement the method outlined in Section 3.2, we chose to write corresponding code in the language Python. The references for the method, [1, 28] have not provided the code necessary for computing the eigenvalues, and as such we had to develop everything entirely from scratch. Using the points found in the domain, alongside their images, it was then necessary to filter the points, before we fed them into the functions. Namely, we filter the points within a band of ρ values, ensuring that they satisfy certain criteria.

4.2.1 Filtering Points

To ensure we can indeed find the right points, we sample ≈ 10000 within the domain. We compute the average distance from the origin in the covering space of all of the available points, and feed them into an algorithm we designed in order to compute two quantities, the

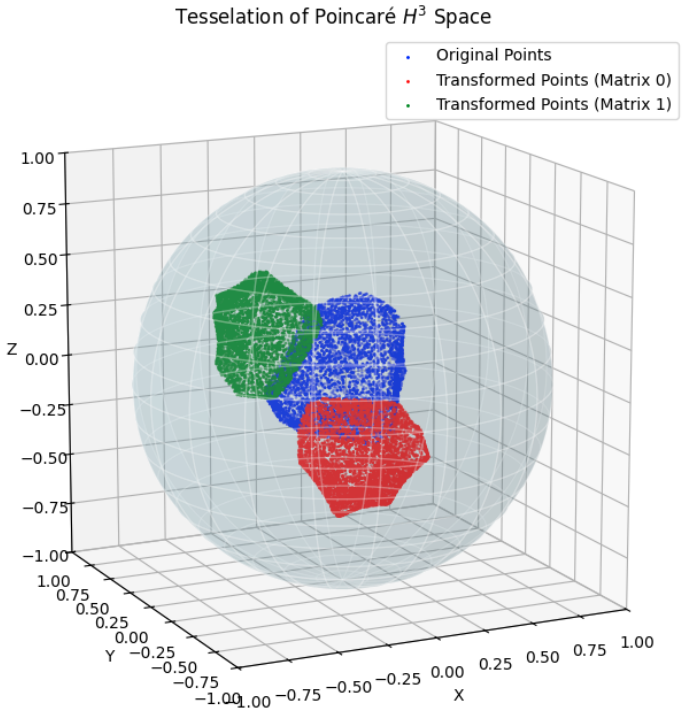

Figure 9: An example of the tessellation of space in the Poincaré model for $m188(-1, 1)$.

$\rho_{\max}$ previously mentioned, and a $\rho_{\min}$. Starting from the average distance of all the points, we iteratively increase and decrease the band of distances considered in order to meet the requirement of the number of rows dictated by the specific value of k we have chosen, and moreover to meet the minimum images requirement we have also set, such that for all the points $n_i > u$ for some $u \in \{1, 2 \ldots, |\Gamma|\}$.

Running through the outline of algorithm 1, we first compute the target number of rows and columns we wish to have, given the specification for L and c. Since both parameters are functions of k, we use the `compute_target_M`(L, c) function to compute the rows M_{desired} and columns N. Next, we set $\rho_{\min} = \rho_{\max} = \rho_{\text{avg}}$, to the average distance of all of the points as a starting point. Then, the algorithm iterates by increasing and decreasing both the $\rho_{\min}$ and $\rho_{\max}$ by checking how far off the current number of rows is from the desired. The `process_images`() function is responsible for calculating the size of the matrix that would be created using the points in the current iteration of the loop. The expansion and reduction of the range is done dynamically according to the size of the over/under-shoot of the current number of rows from the desired, as can be seen in algorithm 2. We then run a final check by using a binary search through the final list to ensure the compiled points fit the criteria we were looking for.

Indeed, determining the tiling radius like such gives us a selection of points to choose for entry into the matrix. Then, in order to choose which points from this list actually make their way into the final entries we defined a function which computes based on the number of images for each point the final selection. In particular, we make use of the `select_points_for_c`() function to search through the entire dictionary of points outputted by the determine tiling radius function, and bias points with more images as opposed to points with less.

Algorithm 1: Determine Tiling Radius

Input: data_with_distances, L, c, min_images, tolerance, initial_step_size, min_step_size

Output: final_points, $\rho_{\min}$, $\rho_{\max}$, valid_points

```
begin
    Compute M_desired and N using compute_target_M(L, c);
    Initialize ρ_min, ρ_max to the average distance of transformed points;
    Set step_size ← initial_step_size;
    Prepare images_list by sorting transformed points by distance;
    for each iteration until convergence or max iterations do
        Compute total_rows, valid_points using process_images(images_list, ρ_min,
         ρ_max, min_images);
        if total_rows ≥ M_desired then
            if total_rows > 1.1 · M_desired then
                Reduce range of ρ_min, ρ_max and adjust step_size;
            else
                Break the loop;
        else
            Expand range of ρ_min, ρ_max conservatively and adjust step_size;
    Filter points using binary_search_filter to construct final_points;
    return final_points, ρ_min, ρ_max, valid_points;
```

4.2.2 Computing Special Functions and Matrix Construction

In order to optimize computational time spent on evaluating the special functions outlined in 3.2, we used a process of vectorization, inputting the values needed to be evaluated as vectors. The building and construction of the matrix takes the most amount of time, as very little is known as to the fast computation of hyperspherical bessel functions. The reference [27] indeed provides a method for this fast computation for a high range of parameters, but unfortunately the code provided in the paper is currently incompatible with our implementation, and hence we could not make use of it. However, for our purposes, we simply coded evaluation of the hyperspherical functions according to (3.8), along with the representation of the legendre function as a product with the hypergeometric function.

Due to the ambiguity in the matrix constructed in [1], which we believe is due to multiple typos, alongside a lack of explanation as to the specific structure, this may be an area in which our implementation is faulty.

Nonetheless, in order to reach computation times which are in time with, and infact faster than in [1], we chose to do all of our computation in parallel, across a wide range of processors. In particular, we made use of the Habrok computing cluster, to split our task across multiple nodes, each of which contains 128 AMD 7763 processors clocked at 2.45GHz, with a total of 128G of memory. We defined an overarching algorithm which uses the already mentioned algorithms above, to compute in parallel across the cluster.

Algorithm 2: Dynamic Adjustment of $\rho_{\min}$ and $\rho_{\max}$

Input : M_{desired}: Target number of rows, initial_step_size, min_step_size
Output: $\rho_{\min}, \rho_{\max}$: Adjusted range

```
Initialize step_size ← initial_step_size;
while True do
    if total_rows ≥ M_desired then
        if total_rows > M_desired × 1.1 then
            step_size ← max(step_size/2, min_step_size);
            ρ_min ← ρ_min + step_size;
            ρ_max ← ρ_max − step_size;
        else
            break;
    else
        ρ_min ← ρ_min − step_size;
        ρ_max ← ρ_max + step_size;
        if total_rows > M_desired × 0.9 then
            step_size ← max(step_size/2, min_step_size);
        else
            step_size ← min(step_size × 1.05, initial_step_size);
```

Algorithm 3: Filter Points for Overconstraint

Input: final_points, data_with_distances, M_{desired}
Output: selected_points, selected_transformed_points, points_images

```
begin
    Compute n_j_values for each point in final_points;
    Select indices using select_points_for_c(n_j_values, M_desired);
    Extract selected points and their transformed versions;
    Construct points_images as tuples of points and their images;
    return selected_points, selected_transformed_points, points_images;
```

To start, we identify a range of k values for which we wish to compute our algorithm over, together with a particular resolution with which we want to do so. Next, we split the task of computation into a number of chunks, each of which will contain a block of k's over which to do the computation. Unfortunately, since every k dictates with it a different over-constraint parameter and L, the sizes of the matrices are not uniform across the range, and thus the computation time to compute the matrices themselves is not uniform. Since the matrices take up the largest chunk of computational effort, this effect would scale quite massively in the whole parallelization, leaving some processors idle while others continue to work.

To make the process more efficient we assign according to the size of the k's, via a round-robin system, each k to a particular chunk, such that the time to compute each node is as uniform as possible.

Algorithm 4: Assign k-Values Uniformly to Chunks and Nodes

Input: k_values: List of k-values, total_chunks: Total number of chunks, num_nodes: Total number of nodes, node_index: Index of the current node
Output: chunks_assigned: Chunks assigned to this node, chunk_indices: Indices of assigned chunks

```
begin
    Initialize empty chunks Initialize k_values_chunks ← [[] for i ∈ [0, total_chunks)];
    for (idx, k_value) in enumerate(k_values) do
        chunk_idx ← idx mod total_chunks;
        Append k_value to k_values_chunks[chunk_idx];
    Initialize chunks_assigned ← [];
    Initialize chunk_indices ← [];
    for i ∈ [0, total_chunks) do
        if i mod num_nodes = node_index then
            Append k_values_chunks[i] to chunks_assigned;
            Append i to chunk_indices;
    return chunks_assigned, chunk_indices;
```

Algorithm 5: Process k-Values Chunk

Input: chunk_index, k_values_chunk, data_with_distances, min_images, tolerance, manifold_name, num_best_to_compute (default: 5)
Output: Processed k-values and corresponding chi-squared values.

```
Initialize variables: chi_squared_values_chunk, k_values_processed, and
 placeholders for intermediate computations;
foreach k_value ∈ k_values_chunk do
    Compute new values c and L based on k_value;
    if c ≠ previous_c_value then
        Determine tiling radius using determine_tiling_radius;
        Compute desired M and N using compute_target_M;
        Filter points for overconstraint using filter_points_for_overconstraint;
        Update intermediate variables: classified_transformed_points,
         selected_points, selected_transformed_points, points_images, and
         previous_c_value;
    Generate matrix system A using generate_matrix_system;
    if A is empty then
        continue to next k_value;
    Solve the system using SVD to compute chi-squared values and singular vectors;
    Store the top num_best_to_compute chi-squared values in
     chi_squared_values_chunk;
    Append k_value to k_values_processed;
return k_values_processed and chi_squared_values_chunk;
```

All that is left to do now is choose the number of nodes and number of processors in each node we want to make use of. For a range of k values in $(0, 10)$ with a resolution of 400, we

found it most efficient to utilize 2 nodes with 100 processors being utilized in each node. To parallelize this entire process and the computation as a whole, we wrote an algorithm which would compute (3.15) given a list of k values, which can be seen in algorithm 5. The function `generate_matrix_system` here simply generates our matrix.

At the beginning of starting to code this process, we had a total cpu time of 05:37:15, and after optimizing further and parallelizing, the final version of our code can compute the χ^2 spectrum for any hyperbolic 3-manifold, available in the census in *SnapPea* in a total time of 00:02:31 [5].

The process of constructing the codebase took quite some time and due to limitations on the available amount of time to write the paper it is very possible to make the computation itself faster by optimizing certain parts further. Writing the code in a lower-level language would have drastic effects on the speed, and perhaps parallelizing certain parts of the code instead of the whole process might produce more efficient results.

4.3 Results

Mirroring the approach in [1], we took as our example manifold the space $m188(-1,1)$. Running our algorithm out to $k = 10$, with parameters set by our discussion in the previous sections, we managed to obtain plots of the χ^2 spectrum of our particular space. We denote f = number of images collected per point/total available images per point. In Figure 10a, we

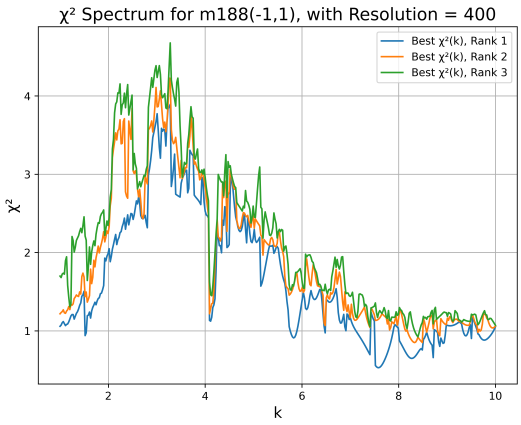

(a) Spectrum of $m188(-1,1)$, $f \approx 0.45$.

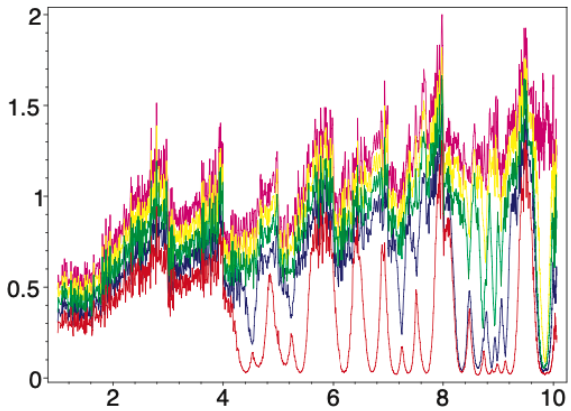

(b) Spectrum of $m188(-1,1)$ as given in [1].

Figure 10: Comparison of spectra for $m188(-1,1)$ between our (a) and [1] (b) algorithm.

plotted the best χ^2 vectors up to 3, and as in [1] we do indeed see that the vectors follow each others behavior. The unfortunate reality of the result is that this does not indeed match the result observed in [1]. The clear and distinct minima seem to be absent from our computations. However we do observe some dips for certain k, these are not near the same dips we observe in the plot available in [1].

Increasing the amount of images we can collect for each point refines the amount of detail

[5] Assuming $k \in (0, 10)$ with a resolution of 400. Small deviations depending on the manifold are possible.

we can obtain from the topology. Indeed this seems to be the case, as we plot ever increasing

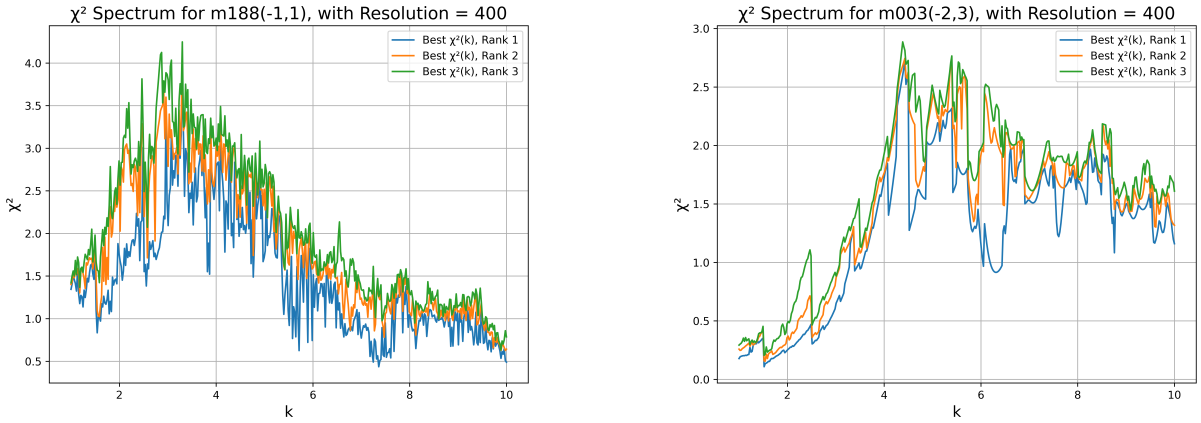

(a) Spectrum of $m188(-1,1)$, $f \approx 0.86$.

(b) Spectrum of $m003(-2,3)$, $f \approx 0.72$.

Figure 11: Comparison of spectra for $m188(-1,1)$ and $m003(-2,3)$ for different f values.

number of images per point, we refine the detail in our spectrum. Meaning perhaps collecting as many images as we can would give maximal chances in computing potential eigenvalues. We provide plots of the space $m003(-2,3)$ as further evidence. Reducing the number of images collected per point also actually slows down the speed of the computations we can make. This is due to the fact that having less images per point results in having to collect more points than we might need necessarily, which results in certain spots of our algorithm, in particular computing the hyperspherical bessel functions and spherical harmonics over many more lists.

5 Conclusion

In this thesis, we have endeavored to explore the profound implications of the universe's topology on the Cosmic Microwave Background (CMB) anisotropies by modeling the universe as a compact hyperbolic manifold. Our objective was to bridge the gap between the abstract mathematical formulations of hyperbolic geometry and their tangible effects on cosmological observations.

The crux of our investigation revolved around the Laplace eigenvalue problem on these manifolds. By solving the Laplace equation we aimed to determine the eigenvalues q^2 corresponding to the vibrational modes that could influence the CMB temperature fluctuations. Utilizing the method of images, or the 'method of ghosts', we constructed eigenfunctions on the manifold by considering contributions from multiple copies of a point under the action of Γ.

Implementing this method presented several challenges. Without access to existing code from prior works, we developed our computational framework from the ground up, coding entirely in Python. We meticulously optimized our algorithms, particularly in computing the hyperspherical Bessel functions and spherical harmonics, which are computationally intensive. Parallelization was a crucial step in enhancing performance, allowing us to distribute computations across multiple processors.

Despite our efforts, reproducing the numerical results from [1] proved to be a formidable task. The lack of detailed explanations and possible ambiguities in the original paper necessitated careful scrutiny of each step in our implementation. While we were able to generate spectra for specific manifolds, such as $m188(-1,1)$ and $m003(-2,3)$, our results did not align with those reported previously. The spectra lacked the clear and distinct minima corresponding to the eigenvalues, suggesting that further refinement of our methods and parameter selection is needed.

An area that warrants additional investigation is the fine-tuning of parameters like the degree of over-constraint c, and the maximum radial coordinate $\rho_{\max}$. These parameters significantly impact the accuracy and convergence of the computed eigenvalues. Future work could focus on developing a more systematic approach to selecting these parameters, potentially improving the alignment of the computed spectra with theoretical predictions.

In conclusion, we explored many aspects of hyperbolic geometry in search of eigenvalues of the Laplace operator on compact hyperbolic spaces. We faced significant challenges in attempts to reproduce the results in [1], given that their code was not available to us and that more importantly their numerical method was not made clear in their paper. We believe that making our code publicly available as open-source software will facilitate future research in this area, as it clearly warrants more investigation and concrete, reproducible results; allowing others to build upon our work and advance the understanding of the universe's large-scale structure.

Bibliography

[1] N. J. Cornish and D. N. Spergel, "On the eigenmodes of compact hyperbolic 3-manifolds," *arXiv preprint arXiv:math/9906017*, 1999.

[2] G. F. Smoot *et al.*, "Structure in the COBE differential microwave radiometer first-year maps," *Astrophysical Journal Letters*, vol. 396, pp. L1–L5, 1992.

[3] C. L. Bennett *et al.*, "First-year wilkinson microwave anisotropy probe (WMAP) observations: Preliminary maps and basic results," *Astrophysical Journal Supplement Series*, vol. 148, pp. 1–27, 2003.

[4] Planck Collaboration, "Planck 2018 results. VI. cosmological parameters," *Astronomy & Astrophysics*, vol. 641, p. A6, 2020.

[5] A. Friedmann, "Über die krümmung des raumes," *Zeitschrift für Physik*, vol. 10, pp. 377–386, 1922.

[6] H. P. Robertson, "Kinematics and world-structure," *Astrophysical Journal*, vol. 82, pp. 284–301, 1935.

[7] G. Lemaître, "The expanding universe," *Monthly Notices of the Royal Astronomical Society*, vol. 91, pp. 490–501, 1931.

[8] A. Einstein, "Die feldgleichungen der gravitation," *Sitzungsberichte der Königlich Preußischen Akademie der Wissenschaften*, pp. 844–847, 1915.

[9] J.-P. Luminet, "The status of cosmic topology after planck data," *Universe*, vol. 2, no. 1, pp. 1–19, 2016. Received: 19 November 2015; Accepted: 07 January 2016; Published: 14 January 2016.

[10] K. Aylor *et al.*, "A comparison of cosmological parameters determined from cmb temperature power spectra from the south pole telescope and the planck satellite," *Astrophysical Journal*, vol. 850, no. 101, 2017.

[11] D. Contreras *et al.*, "Closing in on the large-scale CMB power asymmetry," *arXiv preprint arXiv:1709.10134*, 2017.

[12] R. Aurich, S. Lustig, and F. Steiner, "CMB anisotropy of spherical spaces," *Classical and Quantum Gravity*, vol. 22, no. 17, pp. 3443–3460, 2005.

[13] B. Ryden, *Introduction to Cosmology*. Cambridge University Press, 2 ed., 2016.

[14] J. Stillwell, *Sources of Hyperbolic Geometry*, vol. 10 of *History of Mathematics*. Providence, RI: American Mathematical Society, 1996.

[15] J. M. Lee, *Introduction to Smooth Manifolds*, vol. 218 of *Graduate Texts in Mathematics*. Springer, 2003.

[16] M. Seri, *Analysis on Manifolds*. Bernoulli Institute, 2023. Version 1.2.5 – January 19, 2023. Licensed under Creative Commons Attribution-NonCommercial-ShareAlike 4.0 International.

[17] J. M. Lee, *Introduction to Riemannian Manifolds*, vol. 176 of *Graduate Texts in Mathematics*. Springer Cham, 2 ed., 2019. Originally published with title "Riemannian Manifolds: An Introduction to Curvature".

[18] E. Kim, "Hyperbolic geometry," n.d. Accessed: 2024-12-06.

[19] R. A. Kreek, "Closed curves on hyperbolic manifolds," *Unpublished Manuscript*, August 2007. Retrieved from user-provided document.

[20] J. W. Cannon, W. J. Floyd, R. Kenyon, and W. R. Parry, "Hyperbolic geometry," in *Flavors of Geometry* (S. Levy, ed.), vol. 31, pp. 59–110, Berkeley, California: Mathematical Sciences Research Institute, 1997.

[21] I. Khan, "Hyperbolic geometry: Isometry groups of hyperbolic space," 2012. Unpublished manuscript, available online.

[22] A. F. Beardon, "Hyperbolic geometry," in *The Geometry of Discrete Groups*, pp. 265–292, Berlin, Heidelberg: Springer, 1983.

[23] M. Culler, N. M. Dunfield, M. Goerner, and J. R. Weeks, "SnapPy, a computer program for studying the geometry and topology of 3-manifolds." Available at http://snappy.computop.org (05/12/2024).

[24] F. Bonahon, *Low-Dimensional Geometry: From Euclidean Surfaces to Hyperbolic Knots*, vol. 49 of *Student Mathematical Library*. American Mathematical Society, 2009. Focused on foundational hyperbolic geometry, tessellations, and low-dimensional topology.

[25] A. et al., "Planck 2015 results: XIII. cosmological parameters," *Astronomy & Astrophysics*, vol. 594, p. A13, sep 2016.

[26] N. J. Cornish, D. N. Spergel, and G. D. Starkman, "Does the universe have an odd topology?," *Physical Review D*, vol. 57, no. 10, pp. 5982–5996, 1998.

[27] T. Tram, "Computation of hyperspherical bessel functions," *Global Science Preprint*, 2017. Available at https://github.com/lesgourg/class_public.

[28] N. J. Cornish *et al.*, "Can COBE see the shape of the universe?," *Physical Review Letters*, vol. 80, pp. 181–184, 1998.

Appendix

1: Details of the Separation of Variables and the Associated Ordinary Differential Equations

To provide additional details and derivations related to the separation of variables approach for the Laplace equation (3.4) in the hyperbolic manifold setting, we present here the steps and resulting ordinary differential equations (ODEs).
Starting from the eigenvalue equation

$$(\Delta + q^2)\Psi(\rho, \theta, \phi) = 0, \tag{.1}$$

on the hyperbolic space H^3, we have the Laplace-Beltrami operator in pseudospherical coordinates (ρ, θ, ϕ) given by

$$\Delta = \frac{1}{\sinh^2(\rho)} \left(\Delta^{\rho} + \Delta^{\theta,\phi}\right), \tag{.2}$$

where

$$\Delta^{\theta,\phi} = \frac{1}{\sin(\theta)} \frac{\partial}{\partial\theta} \left(\sin(\theta) \frac{\partial}{\partial\theta}\right) + \frac{1}{\sin^2(\theta)} \frac{\partial^2}{\partial\phi^2} \tag{.3}$$

and

$$\Delta^{\rho} = \frac{\partial}{\partial\rho} \left(\sinh^2(\rho) \frac{\partial}{\partial\rho}\right) \tag{.4}$$

We assume a separable solution of the form

$$\Psi(\rho, \theta, \phi) = X(\rho)\, Y(\theta, \phi). \tag{.5}$$

Inserting (.5) into (.1) yields

$$(\Delta + q^2)(X(\rho)Y(\theta, \phi)) = 0. \tag{.6}$$

Using the expression (.2) for Δ, we have

$$\frac{1}{\sinh^2(\rho)} \left[\frac{d}{d\rho} \left(\sinh^2(\rho) \frac{dX}{d\rho}\right) Y(\theta, \phi) + X(\rho)\Delta_{\theta,\phi} Y(\theta, \phi)\right] + q^2 X(\rho)Y(\theta, \phi) = 0. \tag{.7}$$

Divide both sides of (.7) by $X(\rho)Y(\theta, \phi)$:

$$\frac{1}{\sinh^2(\rho)} \left(\frac{\Delta^{\rho} X}{X} + \frac{\Delta^{\theta,\phi} Y}{Y}\right) = q^2 \tag{.8}$$

Since the left-hand side separates into a ρ-dependent term and a (θ, ϕ)-dependent term, we introduce a separation constant. The angular part yields the well-known spherical harmonics eigenvalue equation:

$$\Delta_{\theta,\phi} Y(\theta, \phi) = -l(l + 1)Y(\theta, \phi), \tag{.9}$$

where $l(l + 1)$ is the eigenvalue associated with the spherical harmonics $Y_{lm}(\theta, \phi)$.
Inserting (.9) back, we get

$$\frac{1}{\sinh^2(\rho)} \frac{d}{d\rho} \big(\sinh^2(\rho) \frac{dX}{d\rho}\big) - \frac{l(l + 1)}{\sinh^2(\rho)} X(\rho) + q^2 X(\rho) = 0. \tag{.10}$$

Radial Equation

The radial ODE is then

$$\partial_\rho^2 X + 2 \cdot \coth(\rho)\partial_\rho X + X \cdot \left(q^2 - \frac{l(l+1)}{\sinh^2(\rho)}\right) = 0 \tag{.11}$$

Switiching from q to the wave number k, defined by

$$k^2 = q^2 - 1. \tag{.12}$$

Rewriting (.11) in terms of k, we obtain a standard form of the radial equation whose solutions are given by the hyperspherical Bessel functions. These solutions, denoted $X_k^l(\rho)$, are known to be

$$X_k^l(\rho) = \sqrt{\frac{N_k^l}{\sinh(\rho)}} P^{-1/2-l}_{-1/2+ik}(\cosh(\rho)), \tag{.13}$$

where $N_k^l = \prod_{0 \le n \le l}(k^2 + n^2)$ and P_ν^μ is the associated Legendre function.

Harmonic Functions

The angular functions $Y(\theta, \phi)$ must satisfy (.9), and these are precisely the spherical harmonics $Y_{lm}(\theta, \phi)$:

$$Y_{lm}(\theta, \phi) = \sqrt{\frac{(2l+1)(l-m)!}{4\pi(l+m)!}}\, P_l^m(\cos\theta) e^{im\phi}, \tag{.14}$$

where P_l^m are the associated Legendre polynomials.

Relevant Code

The code used in this thesis is publicly available at the following repositories:

1. Eigenvalue computation algorithm
2. Dirichlet Domain construction and point selection

The second of the two repositories is used to generate the point data which is entered into the algorithm in the first.